Strengthening Medial Olivocochlear Feedback Reduces the Developmental Impact of Early Noise Exposure

Authors: Valeria C. Castagna[1,2,3], Luis E. Boero[1,2,3], Mariano N. Di Guilmi[1], Paul A. Fuchs[4,5], Amanda M. Lauer[4,5,6], Ana Belén Elgoyhen[1,2] and Maria Eugenia Gomez-Casati[2]

Affiliations:

[1]Instituto de Investigaciones en Ingeniería Genética y Biología Molecular, Dr. Héctor N. Torres, Consejo Nacional de Investigaciones Científicas y Técnicas, 1428 Buenos Aires, Argentina.

[2]Instituto de Farmacología, Facultad de Medicina, Universidad de Buenos Aires, 1121 Buenos Aires, Argentina and Consejo Nacional de Investigaciones Científicas y Técnicas, Argentina.

[3]Universidad de Buenos Aires, Facultad de Ciencias Exactas y Naturales, Departamento de Fisiología y Biología Molecular y Celular, 1428 Buenos Aires, Argentina.

[4]Department of Otolaryngology-Head and Neck Surgery, Johns Hopkins University School of Medicine; Baltimore, Maryland 21205, United States.

[5]Department of Neuroscience, Johns Hopkins University School of Medicine, Baltimore, Maryland 21205, United States.

[6]Center for Functional Anatomy and Evolution, Johns Hopkins University, School of Medicine, Baltimore, Maryland 21205, United States.

Corresponding Author: María Eugenia Gómez-Casati, Ph.D.
Instituto de Farmacología. Facultad de Medicina. Universidad de Buenos Aires.
Address: Paraguay 2155. C1121ABG, Buenos Aires, Argentina.
Phone: 54-11-52853350

E-mail: mgomezcasati@fmed.uba.ar, megomezcasati@gmail.com

Conflict of Interest: The authors declare no competing financial or non-financial interest.

Acknowledgements: This research was supported by Agencia Nacional de Promoción Científica y Técnica (Argentina) to M.E.G-C and NIH Grant R01 DC001508 (P.A.F, A.M.L, A.B.E and M.E.G-C) and the David M. Rubenstein Fund for Hearing Research.

Author Contributions: V.C.C, L.E.B, M.N.D-G, P.A.F, A.M.L, A.B.E and M.E.G-C designed research; V.C.C performed experiments; V.C.C analyzed data. M.E.G-C wrote the paper. All authors discussed the results, read, edited, and commented on the manuscript.

ABSTRACT

The early onset of peripheral deafness significantly disrupts the proper development of the auditory system. Likewise, exposure to loud noise during early development produces a similar disruptive effect. Before hearing onset in altricial mammals, cochlear inner hair cells exhibit spontaneous electrical activity that activates primary afferents and propagates into the central nervous system. This activity is crucial for auditory system maturation and is modulated by the medial olivocochlear efferent (MOC) feedback via α9α10 nicotinic cholinergic receptors present in inner hair cells. In adults, these receptors are restricted to outer hair cells, where they mediate feedback from the MOC system to regulate cochlear amplification. Although the MOC system's protective role to prevent noise-induced hearing loss in adulthood is well-established, its influence during early developmental stages -especially in response to exposure to loud noise- remains largely unexplored. In this study, we examined the effect of the MOC system in the ears of sound-exposed mice during the early postnatal developmental period, by using genetically modified mice - α9 knockout and α9 knock-in models - with either absent or enhanced cholinergic activity. Our findings reveal that both increased and absent olivocochlear activity result in altered auditory sensitivity at the onset of hearing, along with long–range alterations in the number and morphology of ribbon synapses. Furthermore, exposure to loud noise during early development causes long-lasting damage in both wild-type and α9 knockout mice, which lack functional MOC feedback, with effects persisting into adulthood. In contrast, mice with enhanced cholinergic activity were protected from noise-induced damage, with no long-term effects on auditory function. These results highlight the increased susceptibility of the auditory system during early postnatal development. Moreover, they indicate that an enhanced MOC feedback shields the auditory system from noise damage during this period.

INTRODUCTION

The development of the cochlea and the central auditory system is a complex and highly coordinated process, requiring precise timing of cellular and molecular events. During the early postnatal period, several critical changes take place that refine the auditory system's ability to process sound information [1]. Noise exposure during this developmental period can interfere with these processes, impairing the structural organization and signal processing capabilities of the mammalian auditory system and causing lasting damage to cochlear structures and neural circuits [2–6]. Early acoustic exposure affects neuronal sensitivity, innervation, frequency tuning and response characteristics of neurons at multiple levels of the auditory pathway [2,7–11]. Such disruptions can lead to permanent auditory deficits, including reduced sensitivity and impaired sound processing, emphasizing the importance of safeguarding the auditory system during this developmental window.

Cochlear inner hair cells (IHCs) and afferent neurons in altricial mammals exhibit spontaneous electrical activity that propagates into the central nervous system (CNS) prior to the onset of hearing, which occurs around postnatal day 12 (P12) in mice [12–17]. This spontaneous firing is thought to be crucial for promoting neuronal survival in peripheral and central auditory structures, driving their maturation, and shaping their synaptic connections through activity-dependent mechanisms [18–23]. In this postnatal developmental period, medial olivocochlear (MOC) neurons descending from the superior olivary complex in the brainstem make direct synaptic contact with immature IHCs, modulating their spontaneous activity. These MOC neurons form axosomatic synapses through α9α10 nicotinic cholinergic receptors (nAChRs), coupled to Ca^{2+}-dependent SK2 channels, resulting in hyperpolarization of IHCs [24–26]. This transient efferent input is thought to shape burst firing patterns, guiding the normal functional development of IHCs' synaptic machinery and ensuring the establishment of bilateral neural representation in the developing CNS [22,23,27–29]. As IHCs mature, they lose direct efferent contacts and no

longer respond to acetylcholine (ACh). At this stage, MOC fibers extend across the tunnel of Corti and begin forming synapses with OHCs to regulate cochlear amplification [29–34]. The rodent olivocochlear system matures rapidly within the first 2–3 postnatal weeks, with adult-like cochlear innervation patterns established by the end of the first month [30,35–37]. ACh-induced responses in OHCs emerge by P6, shifting from a nicotinic-like current to an outward potassium current around the onset of hearing, even before efferent synapses are fully developed [38,39]. While the protective role of the MOC system in preventing noise-induced hearing loss in adulthood is well-documented [40–44], its impact during early developmental stages, particularly in response to acoustic exposure, remains largely unexplored. Thus, the extent to which ascending and descending pathways interact with the acoustic environment to shape activity patterns and instruct neuronal circuit formation remain largely unknown.

This study explores how the strength of the cholinergic MOC input and early noise exposure affect auditory system development, focusing on the largely unknown effects of noise during this sensitive period. We used genetically modified mice with different levels of α9α10 nAChR activity: α9 knock-out mice (Chrna9 KO; α9KO), which lacks cholinergic transmission between efferent neurons and hair cells [45], and α9 knock-in mice (Chrna9L9'T; α9KI) carrying an α9 point mutation that leads to an enhanced MOC effect [42]. We show that animals genetically engineered to have differences in MOC modulation strength affect the onset of hearing and alter the number and morphology of ribbon synapses in mature IHCs, indicating the importance of normal activity of the cholinergic component of the efferent pathway during postnatal auditory development. Moreover, early-age noise exposure to loud noise produces lasting alterations in auditory sensitivity in wild type (WT), with these effects being more pronounced compared to sound exposure in adulthood [44]. In WT mice, adult noise exposure does not lead to permanent threshold elevations and results in comparatively minor synaptic loss, highlighting the increased susceptibility during postnatal development [44]. In α9KO mice, which lack efferent inhibition,

early-age exposure resulted in a persistent loss of auditory nerve synapses, emphasizing the essential role of the MOC pathway. Conversely, in α9KI mice, where cholinergic efferent inhibition is enhanced, early-age noise exposure does not lead to elevated auditory thresholds or synaptic loss. This protective effect occurs during a critical developmental window when the auditory system is still maturing and olivocochlear terminals are just beginning to establish synapses with OHCs [30,31]. Thus, our work contributes to the evidence that cochlear efferent modulation during postnatal development is essential for establishing normal auditory function. Additionally, we demonstrate that early-age noise exposure can interfere with normal cochlear development and have long-term consequences for function, which can be prevented by enhanced inhibitory input from the MOC system.

RESULTS

Onset of auditory perception in mice with varying levels of efferent inhibition

In this study we used mice with distinct levels of α9α10 nAChR activity: 1) WT, with normal MOC function; 2) α9KO, which lacks cholinergic transmission between MOC neurons and hair cells [45], and 3) α9KI mice carrying an α9 nAChR subunit point mutation that leads to enhanced responses to ACh [42]. To explore the impact of early-age noise exposure, we first identified the optimal developmental stage for introducing such exposure, by assessing the onset of hearing under control (unexposed) conditions in these mouse models. This was done by tracking auditory brainstem responses (ABRs), the sound-evoked potentials generated by neuronal circuits in the ascending auditory pathway, at different postnatal ages across the three groups. Individual ABR waves reflect the activation of auditory periphery and brainstem processing relay stations within the first ~7 ms after sound stimulus onset [46–51]. Wave 1 represents the synchrony in firing of spiral ganglion neurons and is highly correlated with the number of synapses between IHCs and auditory nerve fibers [46,52,53]. Measurements were taken daily from P12 to P16, as well as P22

and P75, in anesthetized mice. Interestingly, we found that ABR onset occurred earlier in α9KI mice, with enhanced MOC function, compared to WT mice with normal MOC synapses and was delayed in α9KO mice lacking α9α10 nAChR activity (Figure 1a and b). Representative ABR traces recorded at P14 in response to a 16 kHz stimulus across varying intensities illustrate differences in ABR thresholds among the three mouse groups with distinct levels of α9α10 nAChR activity (Figure 1a). At this developmental stage, α9KI mice exhibited lower ABR thresholds, and more distinct upward peaks at suprathreshold intensities compared to WT mice. In contrast, α9KO mice showed higher ABR thresholds relative to WT mice (Figure 1a). Figure 1b shows the mean ABR thresholds measured at test frequencies of 11.33, 16, and 22.65 kHz from P12 to P75 across the three groups of mice. A comparison between α9KI and WT mice revealed that α9KI mice displayed measurable ABR responses as early as P13 (Kruskal-Wallis, followed by Dunn's test, degree of freedom [df]= 2, $p = 0.01$ at 22.65 kHz; Figure 1b) and achieved mature threshold levels earlier than their WT littermates (Kruskal-Wallis, followed by Dunn's test, $p = 0.02$ at 16 and 22.65 kHz at P14; Figure 1b). In contrast, ABR onset was delayed by a day in α9KO compared to WT mice (Kruskal-Wallis followed by Dunn's test, df = 2, $p = 0.04$ at 11.33 and 16 kHz; Figure 1b), indicating that cochlear maturation is slower in the absence of pre-hearing efferent modulation. To summarize, at P13, no ABR responses were observed in WT (0 out of 9) or α9KO (0 out of 7) mice in response to tone pips at 80 dB SPL across 11.33, 16, and 22.65 kHz. In contrast, 6 out of 9 α9KI mice exhibited ABR responses at P13. By P14, ABR responses were present in 77.7% of WT mice at 11.33 and 22.65 kHz and in 100% at 16 kHz. Meanwhile, 85% of α9KO mice responded at all frequencies, but with higher thresholds than WT (Figure 1b). All α9KI mice exhibited robust responses at all tested frequencies by P14. By P15, 100% of WT and 91% of α9KO mice showed ABR responses.

Tone pip-evoked ABR wave 1 amplitudes were then analyzed at a suprathreshold level of 80 dB SPL at the different test frequencies in the three groups of mice with varying levels of α9α10

nAChR activity (Figure 2a, b). As illustrated in the representative traces in Figure 2a, measurable ABR wave 1 amplitudes at P13 were only observed in α9KI mice. At P14, the number of discernible upward peaks was fewer in WT and α9KO mice compared to α9KI mice. Up to P15, response peaks at 80 dB SPL were slightly larger and more distinct in α9KI mice, reflecting enhanced auditory responses during this postnatal developmental window. However, starting at P16, α9KI mice exhibited smaller ABR wave 1 amplitudes, with significant differences observed at P75 at 16 and 22.65 kHz compared to WT mice (one way ANOVA followed by Holm-Sidak test, df=2, p=0.03 at both frequencies; Figure 2b). In α9KO mice, wave 1 amplitudes remained smaller than those of WT and α9KI mice until P16, with the difference being significant at 22.65 kHz (one way ANOVA followed by Holm-Sidak test, df = 2, p = 0.02; Figure 2b). These findings align with the ABR threshold results, indicating that the strength of efferent cholinergic inhibition to hair cells contributes to the timely development of auditory function. The reduced ABR wave 1 amplitudes obtained in mature mice with either enhanced or null cholinergic activity indicates that proper MOC modulation during development might be crucial for the correct formation of auditory nerve synapses. Analysis of ABR wave 1 latencies at different postnatal ages showed no significant differences between genotypes (Figure 2c). While wave 1 latencies were consistently longer across all groups at P14, they shortened to levels typical of mature mice by P15.

OHC function was assessed through distortion-product otoacoustic emissions (DPOAE) at the different postnatal ages. In a healthy cochlea, two close pure tones produce distortions due to OHC nonlinearities, which are amplified by OHC electromotility and detected with a microphone in the external ear canal [54,55]. DPOAE responses followed a similar pattern to ABR thresholds, though the differences were not statistically significant (Kruskal-Wallis, df = 2, p > 0.05 at all frequencies; Figure 1c). At P13, DPOAE responses were nearly absent in WT (1 out of 9) and α9KO (0 out of 7) mice across the tested frequencies. In contrast, 3 out of 9 α9KI mice showed DPOAE responses at 16 and 22.65 kHz. By P14, DPOAE responses were observed in 75% of

WT and α9KO mice at 16 and 22.65 kHz, and in 60% of mice at 11.33 kHz. All α9KI mice exhibited strong DPOAE responses at all tested frequencies by P14. By P15, response rates reached 100% in both WT and α9KO mice. Note that at P22 and P75, mean ABR and DPOAE thresholds in α9KI mice were slightly elevated by 5–10 dB compared to WT and α9KO mice (Figure 1b, c). This elevation reached statistical significance only for ABR thresholds at P22 (Kruskal-Wallis, df = 2, p = 0.03 at 11.33 kHz; p = 0.04 at 16 kHz and p = 0.02 at 22.65 kHz). The elevated thresholds in α9KI mice at these mature stages suggest that this may be due to enhanced cholinergic activity on OHCs, as previously reported [42]. Collectively, these findings indicate that the onset of hearing is altered in mice with either absent or enhanced olivocochlear cholinergic feedback. Due to this observation, we decided to expose WT, α9KO, and α9KI mice to loud noise at P15 to test the effects of exposure to increased acoustic stimulation. At this stage, all three genotypes exhibited measurable ABR waveforms, though their wave 1 thresholds differed and had not yet reached mature levels (Figure 1 and 2).

ABR thresholds after early-age noise exposure in mice with different degree of MOC inhibition

To investigate the impact of early-age noise exposure, we exposed WT, α9KO, and α9KI mice to loud noise at P15. This allowed us to evaluate how acoustic experience influences auditory function before full threshold maturation in each genotype. Mice were exposed to 1–16 kHz noise at 100 dB SPL for 1 hour at P15. Auditory responses were then assessed at 1-, 7-, and 60-days post-exposure to track functional changes over time.

Previous studies in WT mice exposed to the same noise protocol at P21 reported a significant increase in auditory thresholds of 10–35 dB SPL one day after exposure, which returned to baseline within a week, indicating a transient threshold shift [44]. In contrast, as shown in Figure 3a, no changes in ABR thresholds were observed at P16, one day after noise exposure,

across frequencies of 8, 16, and 22.65 kHz in WT mice compared to unexposed controls. Remarkably, ABR thresholds at P16 were slightly lower than those measured at P15, prior to noise exposure, and showed no significant difference when compared to unexposed controls at the same age. This suggests that noise did not have an immediate effect on the maturation of auditory thresholds at this postnatal developmental stage. One week after exposure, however, ABR thresholds were elevated at all frequencies in noise-exposed WT animals, and this increase persisted for at least two months post-exposure (Mann- Whitney test, df = 1, P22: $p = 0.006$ at 8 kHz; $p = 0.007$ at 16 kHz; $p = 0.002$ at 22.65 kHz and P75: $p = 0.04$ at 8 kHz; $p = 0.03$ at 16 kHz and $p = 0.04$ at 22.65 kHz; Figure 3a). This outcome contrasts with the transient threshold elevation observed in WT mice, from the same genetic background, exposed at P21 using the same noise protocol [44], suggesting that noise exposure at this early developmental stage produces more detrimental long-term damage.

A similar trend as seen in WT mice was observed after exposing α9KO mice to noise at P15 (Figure 3b). One day after exposure, there were no changes in ABR thresholds at 8, 16 and 22.65 kHz. However, seven days post-exposure, there was an elevation in auditory thresholds across all frequencies (Mann-Whitney test, df = 1, $p = 0.03$ at 8 kHz; $p = 0.01$ at 16 kHz and $p = 0.02$ at 22.65 kHz), which, unlike in WT mice, returned to normal levels after two months (Mann-Whitney test, df = 1, $p > 0.05$ at all frequencies; Figure 3b). Notably, in α9KI mice, ABR thresholds were not affected by noise exposure at all the frequencies tested (Figure 3c), suggesting that even at this early age, the enhancement of cholinergic activity on OHCs provides protection from noise-induced cochlear threshold elevations (Mann-Whitney test, df = 1, $p > 0.05$ at all frequencies).

Amplitudes of cochlear sound-evoked potentials after early-age noise exposure in mice with different degree of efferent inhibition

To assess the neural activity across auditory nerve fibers, we measured ABR wave 1 amplitudes at frequencies of 8, 16, and 22.65 kHz at different ages after noise exposure in the three mouse groups (Figure 4). One day after noise exposure, we observed a reduction in wave 1 amplitudes across all frequencies in WT mice. Further testing of WT mice one week and two months post-exposure revealed a significant and long-lasting reduction, indicating a permanent decrease of ABR wave 1 amplitude (Mann- Whitney test, df = 1, P22: $p = 0.007$ at 8 kHz; $p = 0.005$ at 16 kHz; $p = 0.005$ at 22.65 kHz and P75: $p = 0.04$ at 8 kHz; $p = 0.002$ at 16 kHz and $p = 0.002$ at 22.65 kHz; Figure 4a). Similar permanent reductions in wave 1 amplitude were observed in α9KO mice after exposure to noise at 16 and 22.65 kHz (Mann-Whitney test, df = 1, P22: $p = 0.04$ at 16 kHz; $p = 0.001$ at 22.65 kHz and P75: $p = 0.03$ at 16 kHz and $p = 0.04$ at 22.65 kHz; Figure 4b). Notably, no changes in ABR wave 1 amplitudes were observed at any age post-exposure in mice with enhanced α9α10 nAChR activity, suggesting a preservation of cochlear synapses after noise exposure (Mann-Whitney test, df = 1, $p > 0.05$ at all frequencies; Figure 4c).

DPOAE thresholds after early-age noise exposure in mice with different levels of α9α10 nAChR activity

To assess the impact of early-age noise exposure on the function of OHCs, we recorded DPOAEs at 8, 16, and 22.65 kHz on the three groups of mice with varying levels of MOC function (Figure 5). During early development, the auditory system undergoes significant maturation, leading to decreasing DPOAE thresholds with age, as shown in Figure 1c. In WT mice, one day after noise exposure at P16, there was no difference in DPOAE thresholds between the noise-exposed group and unexposed controls (Figure 5a). However, when comparing DPOAE thresholds at P16 to those at P15 within both groups (i.e. exposed and unexposed controls), a clear reduction was observed (Figure 5a). This decline in thresholds underscores the natural maturation process of the auditory system, indicating that early noise exposure does not

immediately disrupt the ongoing development of DPOAE thresholds at this early postnatal stage. By P22, seven days after noise exposure, an increase in DPOAE thresholds was observed that was statistically significant only at 16 kHz (Mann-Whitney, df = 1, p = 0.01; Figure 5a). Yet, two months later, DPOAE thresholds were comparable to those of unexposed WT controls across all tested frequencies, suggesting that early noise exposure did not result in long-term changes in OHC function (Figure 5a).

In α9KO mice, DPOAE thresholds remained unchanged 1 day after noise exposure. However, seven days post-exposure, significant threshold elevations were observed at 8 and 16 kHz, but not at 22.65 kHz (Mann-Whitney, df = 1, p = 0.02 at 8 kHz and p = 0.02 at 16 kHz). After two months, recovery to unexposed levels occurred only at 8 kHz, while DPOAE thresholds remained elevated at 16 kHz (Mann-Whitney, df = 1, p = 0.003 at 16 kHz; Figure 5b). In contrast, mice with enhanced MOC function showed no changes in DPOAE thresholds at any post-exposure time point (Figure 5c), suggesting that early-age noise exposure did not impair the cochlear amplifier function in these mice with enhanced OHC inhibition.

Ribbon synapse changes after early noise exposure in mice with different levels of α9α10 nAChR activity

Histological analysis was performed on cochleae dissected and fixed at P75 in the three groups of mice with varying levels of α9α10 nAChR activity to evaluate the long-term effect of early noise exposure on the density and structure of IHC ribbon synapses. To visualize these ribbon synapses, we performed immunostaining on whole-mount preparations of the organ of Corti with antibodies against CtBP2-Ribeye, a presynaptic ribbon protein [56], and GluA2, an AMPA-type glutamate receptor expressed at the postsynaptic afferent terminal [43,57,58]. Ribbon synapses were identified by the colocalization of CtBP2 and GluA2 puncta at the base of the IHC, as shown in representative confocal images of IHC synapses from apical whole mount organ of

Corti from control (unexposed) WT, α9KO, and α9KI mice (Supplementary Figure 1a) [58]. We compared the number of colocalized synaptic markers per IHC across three cochlear regions, each representing a distinct frequency range: apex (~4–12 kHz), middle turn (~12–20 kHz), base (~22–40 kHz) (Supplementary Figure 1b). In the low-frequency apical end, both unexposed α9KO and unexposed α9KI mice showed a significant decrease in synaptic density compared to WT, reduced 30.64% and 27.94%, respectively (Kruskal-Wallis, df=2, $p<0.0001$ for both groups; Supplementary Figure 1b, left panel). In the middle region, the reduction was significant only in α9KI mice, with a 35.97% decrease compared to WT (Kruskal-Wallis, df = 2, $p < 0.0001$; Supplementary Figure 1b, middle panel). Similarly, in the high-frequency basal region, synaptic puncta were significantly reduced only in α9KI mice, showing a 22.07% decrease relative to WT (Kruskal-Wallis, df = 2, $p = 0.02$; Supplementary Figure 1b, right panel). We further quantified the volume of CtBP2 puncta and GluA2 receptor patches in these colocalized synaptic markers (Supplementary Figure 1c, d). In the apical region, both α9KO and α9KI mice showed reduced ribbon volumes compared to WT (one way ANOVA followed by Holm-Sidak test, df = 2, $p < 0.0001$ for both groups; Supplementary Figure 1c, left panel). In the middle region, the reduction was significant only in α9KI mice compared to WT (one way ANOVA followed by Holm-Sidak test, df = 2, $p < 0.0001$; Supplementary Figure 1c, middle panel). Interestingly, in the basal region, α9KO mice had increased CtBP2 volumes, while this was smaller in α9KI mice (one way ANOVA followed by Holm-Sidak test, df = 2, $p < 0.0001$ for both groups; Supplementary Figure 1c, right panel). The size of the GluA2 receptor patches was significantly smaller in the apical region of α9KI mice, with no changes in α9KO mice compared to WT (one way ANOVA followed by Holm-Sidak test, df = 2, $p < 0.0001$; Supplementary Figure 1d, left panel). In the middle region, both α9KO and α9KI mice had smaller GluA2 volumes (one way ANOVA followed by Holm-Sidak test, df = 2, $p < 0.0001$, for both groups; Supplementary Figure 1d, middle panel). In the basal region, α9KO mice had larger GluA2 puncta compared to WT (one way ANOVA followed by Holm-Sidak

test, df = 2, $p < 0.0001$; Supplementary Figure 1d, right panel). These results suggest that inhibitory input from cholinergic efferent fibers plays a key role in shaping synaptic density and maintaining the long-term morphology of pre- and postsynaptic elements necessary for optimal auditory function.

The long-term impact of early-age noise exposure on auditory nerve synapse numbers is illustrated in Figure 6, on cochleae dissected and fixed at P75 from control and noise-exposed mice with varying levels of α9α10 nAChR activity. Presynaptic, postsynaptic, and colocalized synaptic puncta quantifications are shown for the apical, middle, and basal cochlear regions (Figure 6, violin plots, right panels). In WT exposed ears, the number of CtBP2, GluA2, and colocalized synaptic puncta significantly decreased at both the apical and basal cochlear ends (Figure 6a). The decrease in CtBP2 puncta was more pronounced in the high-frequency basal region, with a 37.2% decrease compared to controls (Mann-Whitney, df = 1, $p < 0.0001$ at the apical and basal regions). Similarly, GluA2 postsynaptic receptors were reduced in both the apical and basal turns in the cochlea of noise-exposed WT mice (Mann-Whitney, df = 1, $p < 0.0001$ at both cochlear regions). Putative ribbon synapse counts, defined by juxtaposed CtBP2- and GluA2-positive puncta, showed a 34.21% reduction in the apical and a 32.56% reduction in the basal turn following acoustic trauma (Mann-Whitney, df = 1, $p < 0.0001$ at both cochlear regions) (Figure 6a, right panel). In α9KO mice, there was also a reduction in the number of presynaptic, postsynaptic, and colocalized puncta after noise exposure, depending on cochlear frequency/location (Figure 6b). Ribbon puncta in α9KO exposed ears were reduced by up to 14.73% of the control in the apical and 24.75% in the basal cochlear ends after noise exposure (Mann-Whitney, df = 1, $p = 0.001$ and $p = 0.002$ at the apical and basal region, respectively). GluA2-positive postsynaptic receptor patches decreased by 24.79% in the basal turn of noise-exposed mice (Mann-Whitney, df = 1, $p = 0.004$). Following noise exposure, synaptic puncta were reduced by 26.17% in the apical cochlear region and 25.87% in the basal region (Mann-Whitney,

df = 1, p = 0.002 and p < 0.0001 at the apical and basal region, respectively) (Figure 6b, right panel). Interestingly, after two months post-exposure, α9KI ears exhibited no significant changes in presynaptic ribbons, postsynaptic GluA2 receptor patches, or putative synapses across all cochlear regions (Figure 6c). Although not statistically significant, a modest increase in synaptic density (~19% at the basal region) was observed in α9KI tissue (Figure 6c, right panel).

Finally, we quantified the volume of ribbons and AMPA receptor patches (i.e., colocalized CtBP2 and GluA2 puncta) in unexposed and exposed mice with different levels of MOC feedback (Figure 7). In WT mice, noise exposure resulted in significantly larger ribbon volumes in the basal end of the cochlea compared to unexposed mice, with no corresponding changes in AMPA receptor patch size (t-test, df = 1, p = 0.01; Figure 7a). No changes were observed in the apical or middle cochlear regions (Figure 7a). Conversely, α9KO mice showed reduced volumes of both ribbons and AMPA receptor patches in the basal region following noise exposure, with no changes in the apical or middle regions (t-test, df = 1, p = 0.002 for CtbP2 volume and p = 0.003 for GluA2 volume; Figure 7b). Notably, α9KI mice showed no morphological changes, suggesting that enhanced α9α10 nAChR activity protects synapses from noise-induced alterations (Figure 7c).

DISCUSSION

Auditory development is a gradual process that begins during embryonic stages and continues through sensitive postnatal periods. While much is known about the detrimental effects of noise exposure at mature stages, less is understood about its impact during this crucial developmental window and the role of the MOC system in this context. Here, we explored how varying levels of MOC inhibitory modulation affect the developmental consequences of early-age noise exposure. Our findings reveal that changes in the strength of MOC inhibition impact the timing of hearing onset and are crucial for the long-term maintenance of IHC ribbon synapses.

Moreover, loud noise exposure during postnatal developmental stages caused long-lasting changes in auditory sensitivity in WT, highlighting the greater vulnerability of the auditory system to noise-induced injury during early development. Notably, enhanced cholinergic activity in α9KI mice conferred protection from early developmental noise-induced threshold shifts and cochlear synaptopathy. This underscores the crucial protective role of the MOC system during these vulnerable early developmental stages.

Before hearing begins, MOC synapses modulate IHCs' activity, shaping the developmental increase in Ca^{2+} sensitivity of glutamate release at IHC ribbon synapses [16,24,27,59]. Previous work in genetically modified mice and studies involving neonatal transection of the olivocochlear bundle have shown that MOC modulation at these early ages is essential for cochlear maturation, sensory map formation, and synaptic refinement along the auditory pathway [22,23,27,29,60–62]. Our findings further demonstrate that α9α10 nAChR activity regulates hearing onset and synaptic integrity. Enhanced α9α10 nAChR activity in α9KI mice accelerates the onset of hearing, with sound-evoked potentials detected earlier than in mice with normal MOC synapses. In the absence of MOC activity, as in α9KO mice, hearing onset is delayed, with higher ABR thresholds and diminished wave 1 amplitudes compared to WT during early development. Consistent with these findings, recent research on α9KO mice has shown that auditory sensitivity at hearing onset is impaired in the absence of pre-hearing efferent input [28]. In addition, our work shows that both enhanced and absent MOC inhibition interfere with the proper formation and maintenance of ribbon synapses in adult IHCs. At P75, both α9KO and α9KI mice exhibit significant reductions in ribbon synapse density and alterations in the volume of pre- and post-synaptic puncta compared to age-matched WT controls, underscoring the critical role of balanced MOC activity in auditory system development and synaptic organization. In α9KI mice, ribbon and GluA2 patch volumes were reduced, while α9KO mice showed region-specific effects: decreased ribbon volume in the apical region without changes in GluA2 receptor size and

increased synaptic component size in the basal region. Previous studies have emphasized the functional importance of ribbon size, showing that it is tightly regulated by presynaptic Ca^{2+} channels, with alterations in Ca^{2+} influx impacting synaptic plasticity, neurotransmitter release, and active zone maturation [62–65]. During early development, IHC active zones undergo substantial structural and functional maturation, including the removal of extrasynaptic Ca^{2+} channels and the co-localization of glutamate receptor patches with presynaptic ribbons [66–68]. This maturation refines presynaptic morphology, reduces the number of ribbons per synapse, and establishes monosynaptic connections between IHCs and auditory nerve fibers [69–72]. Recent work also suggests that fusion of synaptically anchored ribbons during this period is critical for the development of mature active zones and sustained neurotransmitter release [66]. Given our observation of reduced ribbon size in some cochlear regions of α9KI and α9KO mice, we propose that altered MOC modulation strength may disrupt intracellular Ca^{2+} dynamics, which could impair ribbon precursor fusion, thereby impairing active zone maturation. These findings highlight the essential role of MOC synapses in shaping early auditory sensitivity, reinforcing previous suggestions [27] that effective coordination between afferent and efferent inputs is important for regulating spiking activity in the developing auditory pathway. This coordination is crucial for proper synaptic and auditory system maturation.

Auditory function in vertebrates matures through a well-defined process, transforming the system from high thresholds and limited frequency discrimination at the onset of hearing to a highly sensitive and precise mechanism capable of resolving frequency differences as small as 1 Hz [73]. Our findings suggest that the WT mouse strain used in the present work aligns with this established maturation pattern, as auditory function recordings from P12 to P75 reveal a clear progression from an immature to a mature state. At the onset of hearing (P14 in our strain of mice), the auditory system shows elevated ABR and DPOAE thresholds, reduced wave 1 amplitudes, and poorly defined later ABR waves, reflecting incomplete functional maturation. Over

the following days, thresholds progressively decreased, reaching mature levels by P22. This maturation is accompanied by a steady increase in ABR wave 1 amplitudes from P15 to P22, underscoring the postnatal refinement period necessary for achieving full auditory sensitivity. Thus, by P15, the time when mice were exposed to high levels of noise, the maturation process is not yet complete. A key finding of this study is that exposure to intense sound during early developmental stages results in significantly more severe consequences compared to exposure at a later age [44]. In WT mice, exposure to 100 dB SPL noise for 1 hour at P15 resulted in lasting ABR threshold elevations for up to two months, accompanied by a 35% loss of ribbon synapses. In contrast, the same exposure at P21 causes only transient threshold shifts, which returns to baseline within seven days, with a less pronounced degree of cochlear synaptopathy [44]. This stark difference underscores the heightened vulnerability of the auditory system during early development and highlights the age-dependent impact of noise exposure. Previous reports have also shown that the same scheme of intense noise exposure causes more severe damage in juvenile animals at 4 weeks of age compared to adult animals at 16 weeks of age [74–76]. Although the underlying mechanisms that drive this heightened sensitivity are not known, we can speculate that this increased sensitivity reflects a critical window in which MOC synaptic activity is still maturing or being functionally reinforced. Alternatively, central mechanisms—such as refinement of MOC neurons, completion of myelination, or strengthening of afferent drive—may contribute to the vulnerability observed at this stage. Ongoing maturation of the auditory nerve–lateral olivocochlear (LOC) complex may also play a role, potentially rendering the system more susceptible to disruption by acoustic overexposure during this period. DPOAE thresholds were also elevated seven days post-exposure in WT mice, although these thresholds recovered after two months, suggesting that there is no loss of OHCs or alteration in their function. Given this recovery of DPOAE thresholds but persistently elevated ABR thresholds, we can infer that the elevation is not due to damage in the cochlear amplifier but rather to a deficiency in the afferent

pathway of sound signal transmission. In line with this, the increase in ABR thresholds was accompanied by a reduction in wave 1 amplitudes, which also persisted for two months after noise exposure. This study represents the first report of sustained ABR threshold elevation for such an extended period following moderate noise exposure at 100 dB SPL for 1 hour. Similar results were obtained in 14-day-old rats exposed to a higher noise level of 125 dB SPL for 25 minutes, where after two months post-exposure, elevated thresholds at high frequencies and a loss of presynaptic elements (CTBP2/Ribeye) were observed [77]. Our findings demonstrate a significant loss of ribbon synapses in the apical and basal regions of the cochlea in WT mice following noise exposure, which correlates with decreased ABR wave 1 amplitudes. In addition to cochlear synaptopathy, we observed that IHCs of noise-exposed mice tend to have larger ribbons (Ribeye/CtBP2 volume) compared to unexposed IHCs in the basal region of the cochlea. A similar increase in the volume of presynaptic elements following acoustic trauma was observed using both the RIBEYE-tagRFP mouse model [78] and volume electron microscopy [76]. The observed ribbon enlargement in WT mice may be attributed to the fusion of individual ribbons after noise exposure. In fact, recent evidence indicates an increase in multi-ribbon active zones as well as movement suggesting unanchoring from synaptic tethers in synaptopathic ears [76,78,79]. While the functional significance of this structural adaptation remains unclear, multi-ribbon active zones persist into adulthood [66,67] and are a hallmark of cochlear aging [80], with larger ribbons being associated with increased Ca^{2+}-dependent exocytotic activity [81]. Notably, noise exposure has also been associated with enhanced exocytosis in IHCs, along with an increase in tone-burst responses in auditory nerve fibers [82,83]. A recent study also demonstrated that intense noise exposure (98 dB SPL for two hours) in young animals reduces the number of presynaptic ribbons in OHCs, while increasing the volume and mobility of those that remain [84]. We can hypothesize that ribbon volume enlargement may act as a compensatory mechanism to maintain auditory sensitivity after synapse loss. Importantly, we did not detect changes in the size of GluA2 receptor

patches in WT mice post-noise exposure.

In α9KO mice, which lack α9α10 nAChR activity, elevated ABR and DPOAE thresholds were observed one week after noise exposure at P15, consistent with findings from noise-exposed α9KO mice at P21 [44]. However, in contrast to WT animals, ABR thresholds in α9KO mice nearly fully recovered to unexposed control levels two months post-exposure. While DPOAE thresholds returned to control levels at 8 and 22.65 kHz, they remained elevated at 16 kHz after two months. This elevation in DPOAE thresholds at 16 kHz was accompanied by a slight, though not statistically significant, elevation in ABR thresholds at the same frequency. The recovery of ABR thresholds in α9KO mice, compared to the permanent threshold elevation seen in WT mice, may be attributed to the reduced auditory sensitivity at hearing onset in α9KO mice due to the absence of prehearing efferent modulation. While ABR thresholds return to pre-exposure values, a persistent reduction in wave 1 amplitudes and ribbon synapse counts per IHC was observed. Prior studies suggest that suprathreshold response deficits following noise exposure are driven by the selective loss of high-threshold, low-spontaneous-rate auditory nerve fibers [85]. Accordingly, the lack of threshold elevation despite synaptic loss may reflect the preferential vulnerability of this specific neuronal subpopulation. However, in α9KO ears exposed to noise, both pre- and postsynaptic puncta showed a reduction in size, indicating noise may also involve maladaptive alterations in both pre- and postsynaptic structures.

In contrast to the findings in WT and α9KO mice, α9KI mice, which exhibit enhanced α9α10 nAChR activity, showed no ABR or DPOAE threshold elevations following sound exposure. Additionally, no evidence of cochlear synaptopathy was detected in these mice. This phenomenon had already been described in adult mice (P21) exposed to the same level of noise [44]. At birth, rodent MOC neurons initially innervate IHCs, and by P10, they expand to innervate both IHCs and OHCs. After the onset of hearing, their innervation becomes confined to OHCs, gradually retracting from IHCs [30]. Our results therefore suggest that even with early developmental noise

exposure—when MOC innervation to OHCs is still developing—enhanced α9α10 nAChR responses can effectively exert a protective effect on OHCs against functional and structural damage associated with acoustic trauma. Importantly, our findings also reveal that mice with enhanced α9α10 nAChR activity showed a modest increase in ribbon synapse density following acoustic overexposure. This is consistent with previous work, which documented a more substantial increase in synaptic density in α9KI mice exposed to the same noise protocol at P21 [44]. These results indicate that enhancement of the cholinergic component of the MOC system may support synapse formation following noise exposure.

In summary, this work highlights three key findings: 1) the MOC system plays a crucial role in regulating the development of ribbon synapse density and size, which is essential for proper hearing onset; 2) exposure to loud noise during early development results in more severe auditory consequences compared to the same exposure later in life; and 3) enhancing α9α10 nAChR responses during early development protects against noise-induced damage, underscoring the importance of timely modulation of this receptor post-hearing onset to mitigate developmental impairments.

Clinical implications:

Clinical evidence indicates that early acoustic exposure can adversely affect auditory development, a concern particularly evident in neonates requiring prolonged hospitalization. Advances in newborn hearing screening have revealed a higher-than-anticipated prevalence of auditory neuropathy, especially among infants treated in neonatal intensive care units (NICUs), where persistent high noise levels are common [86,87]. Our experimental findings align with these clinical observations, showing that early-age noise exposure exacerbates auditory deficits in mice. Importantly, enhancement of α9α10 nAChR signaling during early development attenuated noise-induced damage, underscoring the receptor's protective role during a sensitive window of auditory

system maturation. These results offer proof-of-principle for the potential of pharmacological strategies targeting α9α10 nAChRs to prevent developmental hearing loss associated with early acoustic stress.

FIGURES

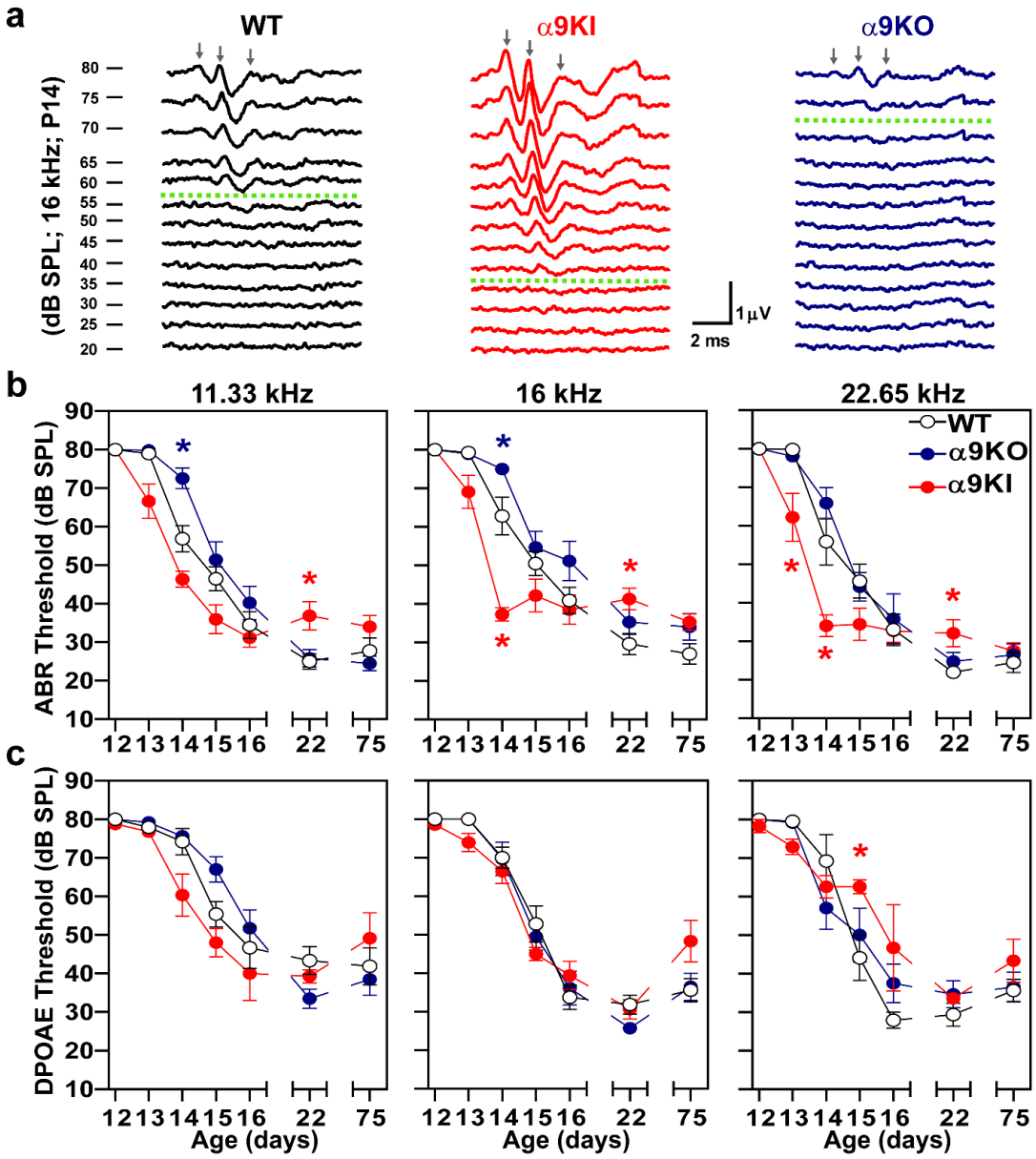

Figure 1: Auditory function in WT, α9KO, and α9KI mice across different postnatal ages. (**a**) Representative ABR waveforms from WT (black), α9KI (red), and α9KO (blue) mice recorded at P14 in response to 16 kHz tone bursts at increasing sound pressure levels (dB SPL). Thresholds, defined by the presence of wave 1, are marked by green dashed traces. Waves 1, 2 and 3 are indicated by gray arrows. The scale bar applies to all three recordings. (**b**) Mean ABR thresholds from P12 to P75 in WT (n = 12), α9KO (n = 14), and α9KI (n = 14) mice at 11.33, 16, and 22.65 kHz. ABR waveforms first became detectable at P13 in α9KI mice, at P14 in WT mice, and between P14 and P15 in α9KO mice. (**c**) Mean DPOAE thresholds from P12 to P75 in WT (n = 12), α9KO (n = 14) and α9KI (n = 14) mice at 11.33, 16 and 22.65 kHz. DPOAE thresholds showed the same trend as ABR only at 11.33 kHz. Group means ± SEM are shown. Red asterisks represent the statistical significance of α9KI compared with WT**,** and blue asterisks represent the statistical significance of α9KO compared with WT (Kruskal-Wallis followed by post hoc Dunn test, *$p < 0.05$).

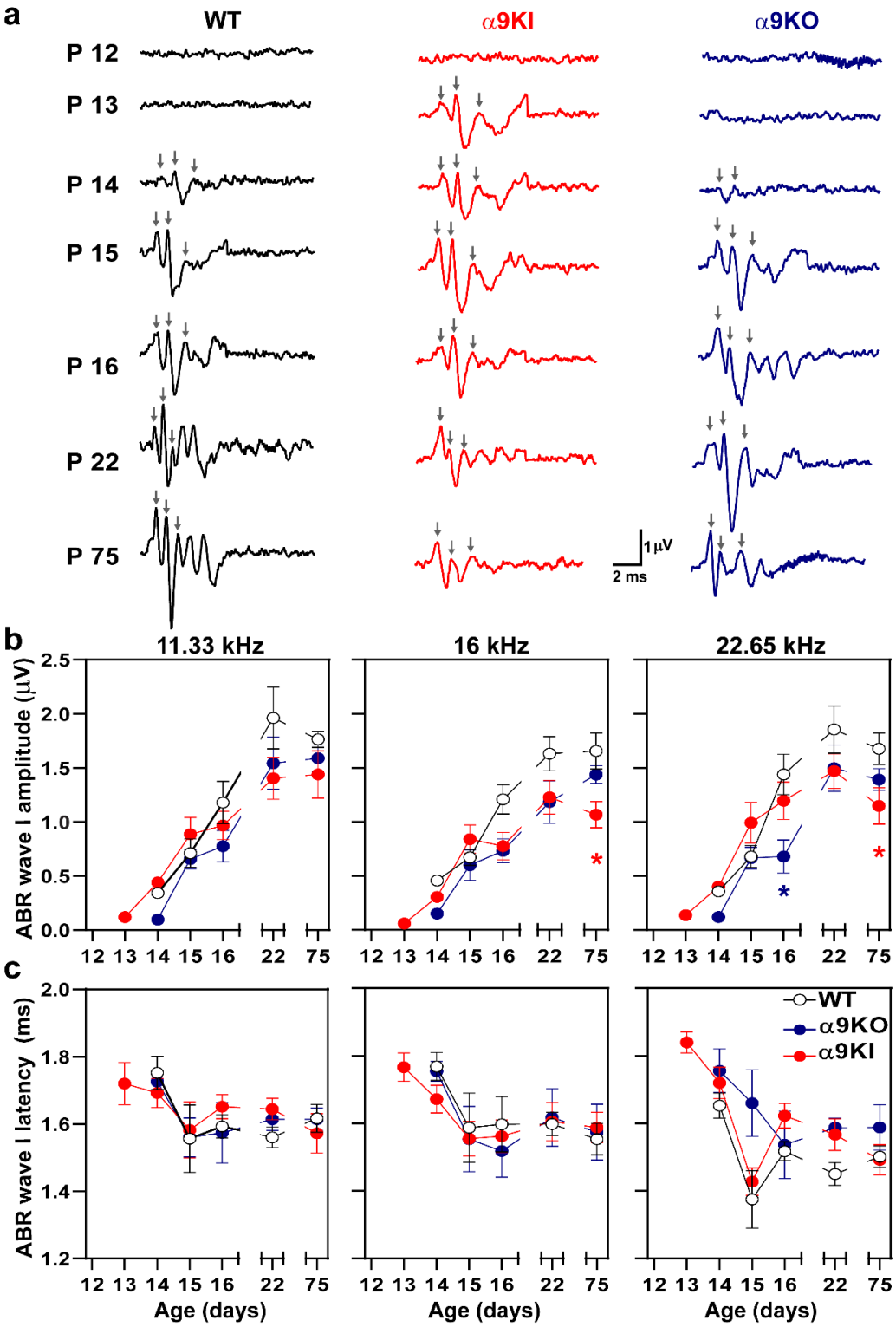

Figure 2: Suprathreshold ABR wave1 amplitudes and latencies in WT, α9KO, and α9KI mice during postnatal development. (**a**) Representative examples of ABR waveforms recorded at 16 kHz, 80 dB SPL, from WT (black), α9KI (red), and α9KO (blue) mice. Waves 1, 2 and 3 are indicated by gray arrows. Each column illustrates waveform maturation across developmental

stages (P12–P16, P22, P75) for each genotype. At P13, α9KI mice exhibit measurable responses, while distinct ABR waves emerge in WT and α9KO mice by P14. Waveform morphology stabilizes by P22 and remains consistent through P75. Scale bars apply to all traces. (**b**) ABR wave 1 amplitudes (μV) at 80 dB SPL for 11.33, 16, and 22.65 kHz across developmental ages in WT, α9KO, and α9KI mice. Amplitudes were measured as the difference between the maximum and minimum peaks. No values are shown for P12 due to the absence of discernible waves. (**c**) ABR wave 1 latencies (ms) at the same frequencies. A developmental decrease in latency is observed between P14 and P15 in all genotypes, though not statistically significant. Data represent mean ± SEM. Red asterisks denote significant differences between α9KI and WT; blue asterisks indicate significant differences between α9KO and WT (one-way ANOVA followed by Holm-Sidak test, *$p < 0.05$; **$p < 0.01$).

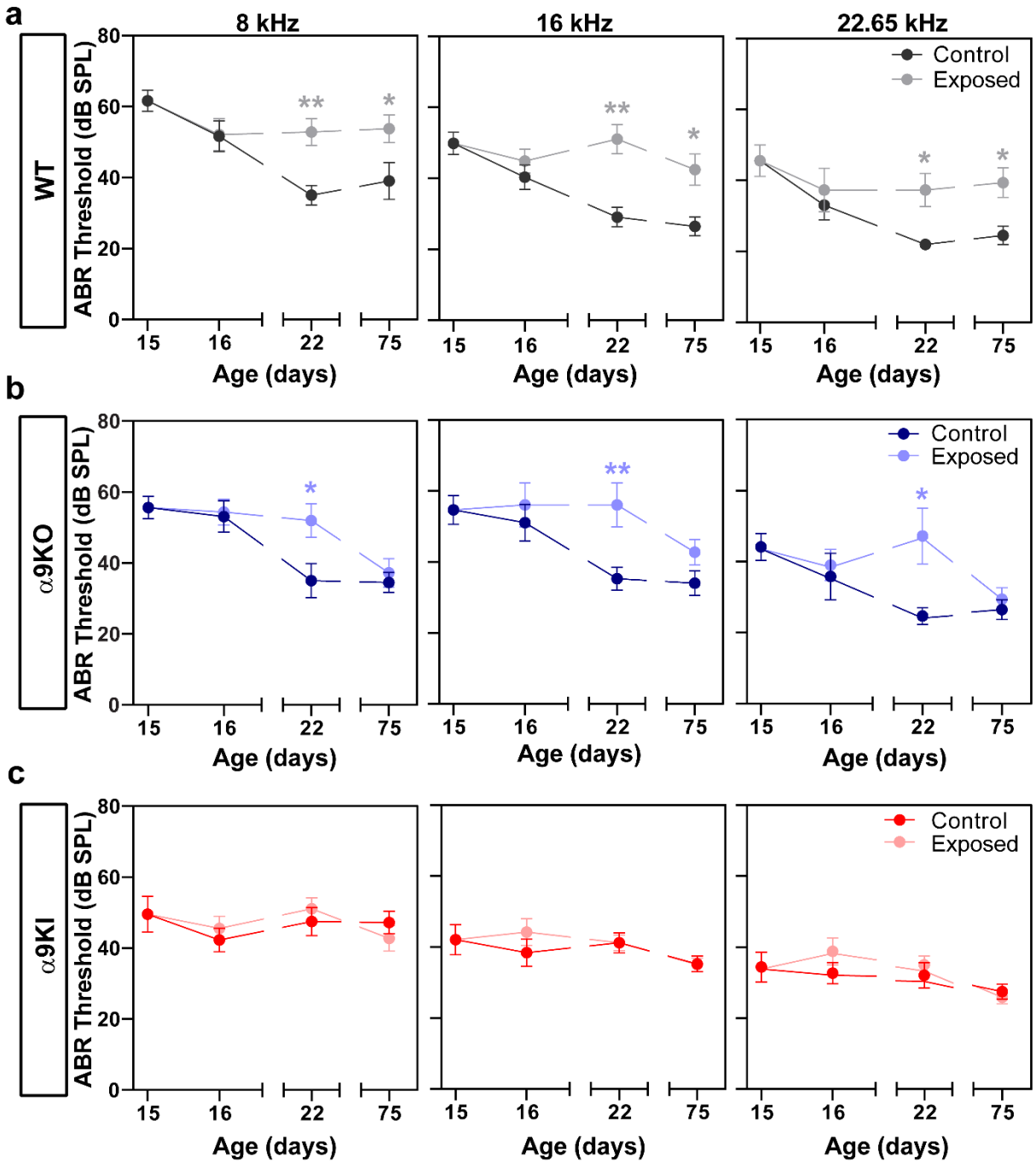

Figure 3: ABR wave 1 threshold measurements in control and noise-exposed WT, α9KO, and α9KI mice at different postnatal ages. ABR thresholds before and after exposure to noise at P15 in WT ($n_{control}$ = 14 and $n_{Exposed}$ = 12) (**a**), α9KO ($n_{control}$ = 11 and $n_{Exposed}$ = 11) (**b**), and α9KI ($n_{control}$ = 12 and $n_{Exposed}$ = 12) (**c**) mice at 8, 16 and 22.65 kHz. WT mice showed a significant increase in ABR thresholds 1 week and 2 months after exposure to noise, indicating a permanent threshold elevation. A recovery of ABR thresholds was observed in α9KO mice 2 months after exposure to noise. α9KI mice did not present any changes in ABR thresholds at any time after acoustic trauma. Each point represents the mean ± SEM. Asterisks represent the statistical significance (Mann-Whitney test, *$p < 0.05$; **$p < 0.01$).

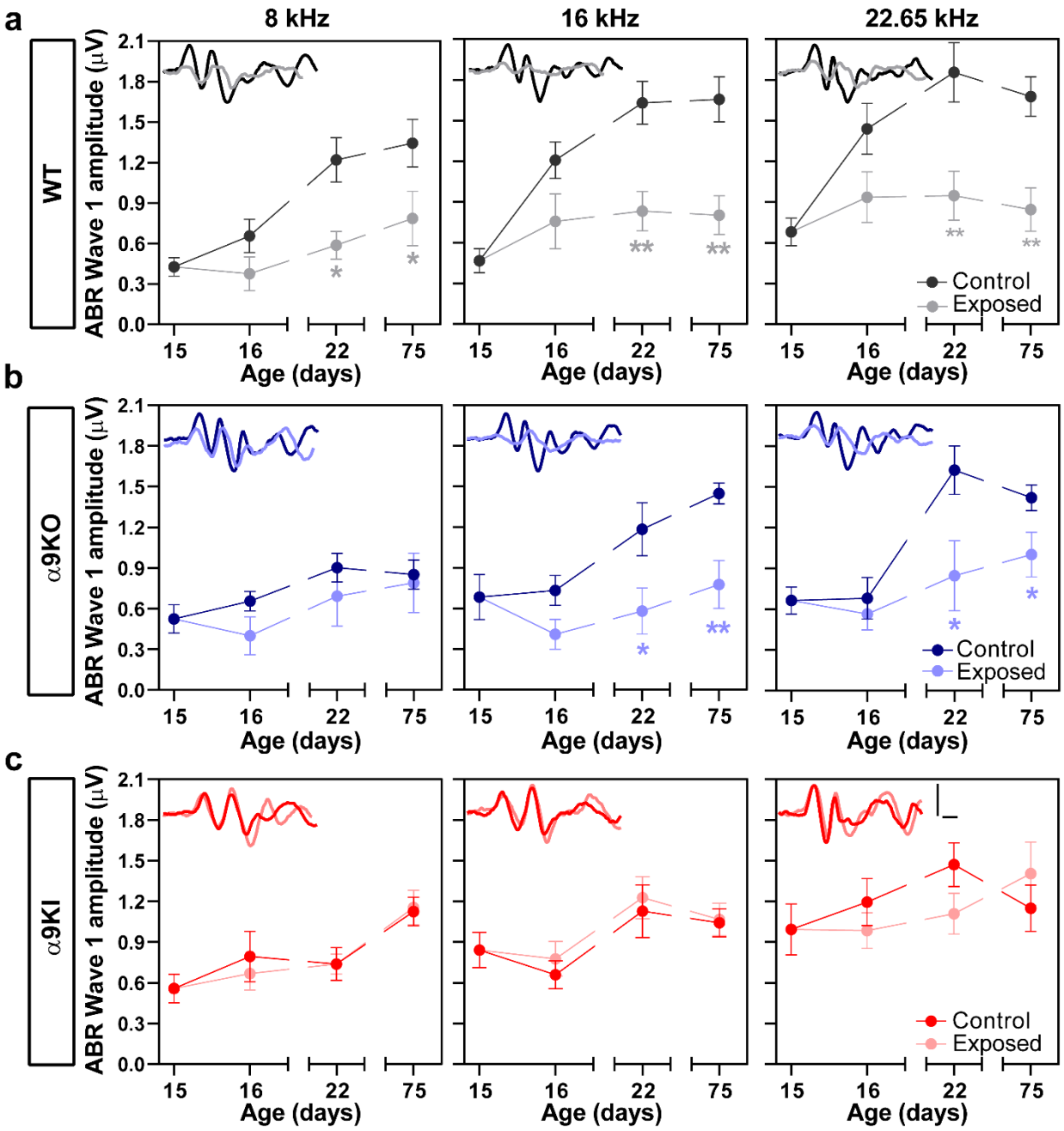

Figure 4: Suprathreshold response amplitude for ABR wave 1 after P15 noise exposure in WT, α9KO, and α9KI mice at different postnatal ages compared to unexposed controls. ABR wave 1 amplitudes (in μV) at 80 dB SPL at 8, 16 and 22.65 kHz in WT ($n_{Control}$ = 14 and $n_{Exposed}$ = 12) (**a**), α9KO ($n_{Control}$ = 11 and $n_{Exposed}$ = 11) (**b**), and α9KI ($n_{Control}$ = 12 and $n_{Exposed}$ = 12) (**c**) mice at the same time points shown in Figure 3. Each panel inset displays representative ABR waveforms recorded at 80 dB SPL for the corresponding frequency, shown for all groups at P75. Scale bars (1 μV vertical, 1 ms horizontal) apply to all traces. WT and α9KO mice exhibited reduced ABR wave 1 amplitudes following noise exposure, whereas wave 1 amplitudes in α9KI mice remained unaffected. Data are presented as mean ± SEM. Statistical significance is indicated by asterisks (Mann-Whitney test, *$p < 0.05$; **$p < 0.01$).

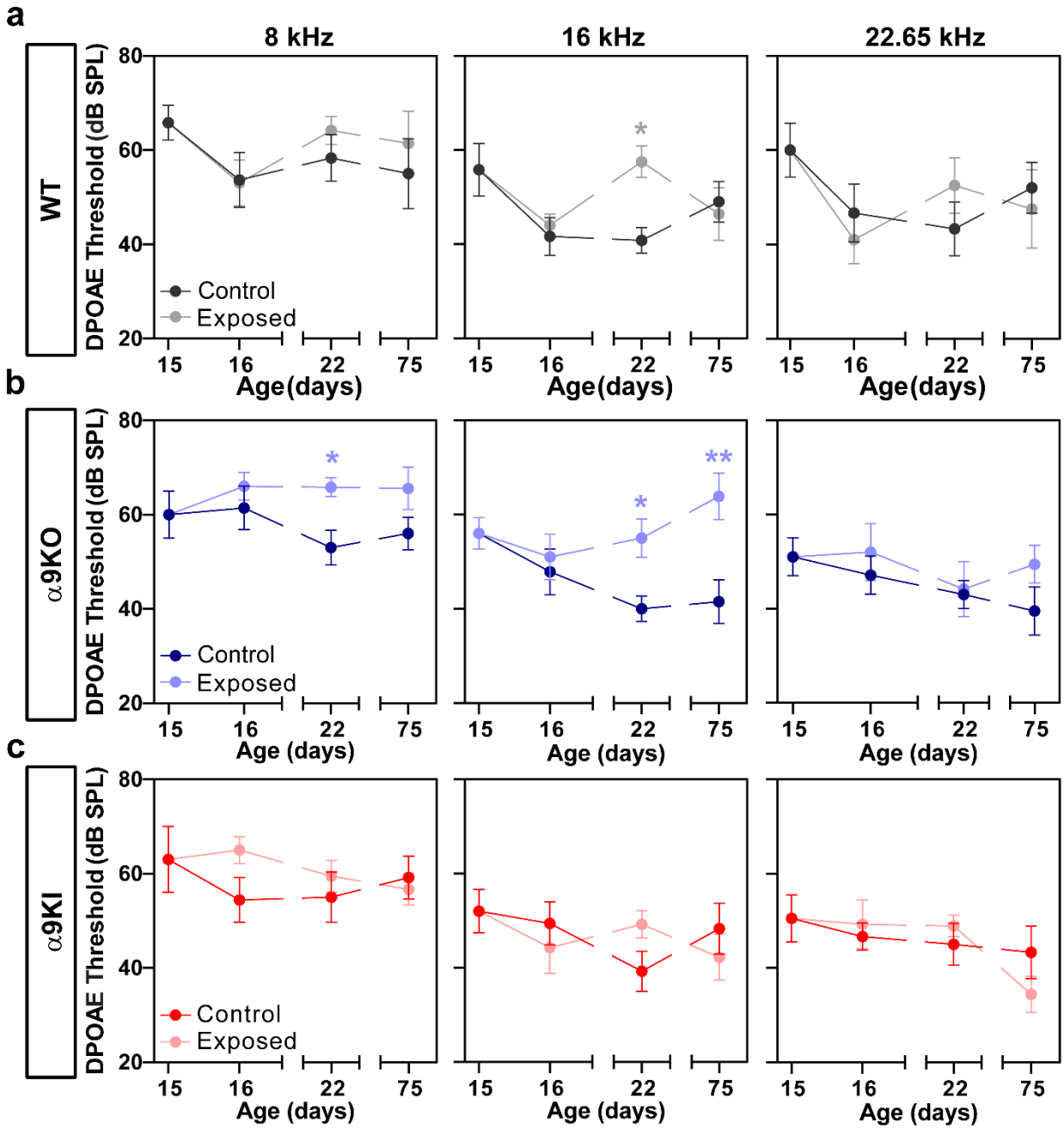

Figure 5: **Assessment of OHC functional integrity at different postnatal ages following noise exposure at P15 in WT, α9KO, and α9KI mice.** DPOAE thresholds are shown for WT ($n_{Control}$ = 14 and $n_{Exposed}$ = 12) (**a**), α9KO ($n_{Control}$ = 11 and $n_{Exposed}$ = 11) (**b**), and α9KI ($n_{Control}$ = 12 and $n_{Exposed}$ = 12) (**c**) at 8, 16 and 22.65 kHz. WT mice exhibited a transient increase in DPOAE thresholds 1 week post-exposure at 16 kHz. α9KO mice showed increased thresholds at 8 and 16 kHz 1 week post-exposure, with sustained elevation at 16 kHz up to 2 months. α9KI mice demonstrated no changes in DPOAE thresholds after noise exposure. Data are presented as mean ± SEM. Statistical significance is indicated by asterisks (Mann-Whitney test, *$p < 0.05$; **$p < 0.01$).

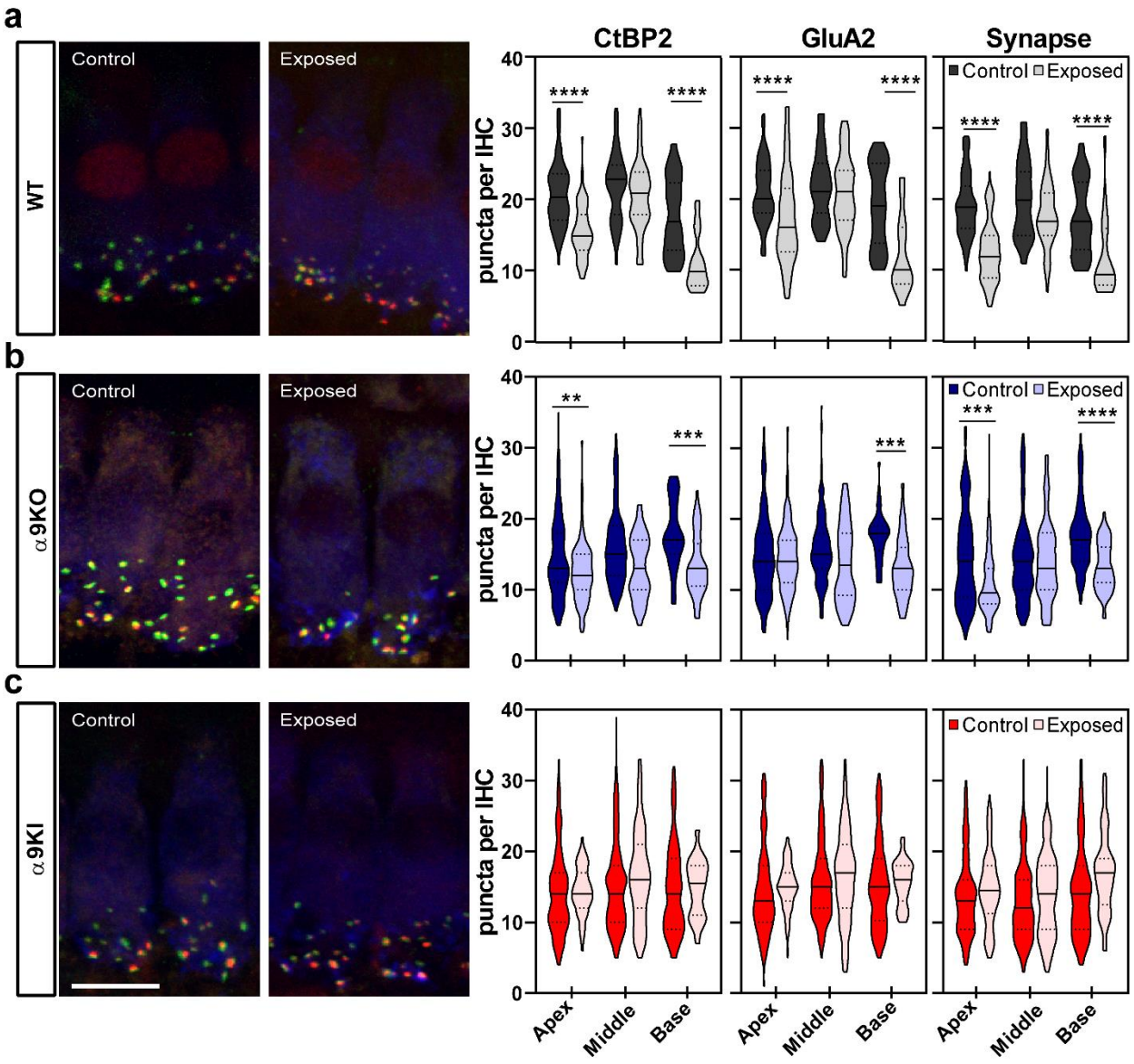

Figure 6: Analysis of the degree of IHC synaptopathy two months after exposure to noise at P15. Left, Representative confocal images of IHC synapses at the apex of the cochlea from cochleae immunolabeled for presynaptic ribbons (CtBP2-red), postsynaptic receptor patches (GluA2-green) and IHCs (Myosin VIIa-blue). CtBP2 antibody also weakly stains IHC nuclei. Scale bar, 10μm. Right, Quantitative data obtained from WT, α9KO, and α9KI mice at P75. For each IHC, we analyzed the number of CtBP2 puncta, postsynaptic GluA2 receptor patches, and putative ribbon synapses. (**a**) In traumatized WT mice, there was a reduction in the number of CtBP2 puncta, GluA2 receptor patches, and putative synapse, at the apical and basal region of the cochlea (WT Control: n_{Apex} = 80 IHC, n_{Middle} = 75 IHC, n_{Base}= 60 IHC; WT Exposed: n_{Apex} = 82 IHC, n_{Middle} = 90 IHC, n_{Base} = 50 IHC). (**b**) In traumatized α9KO mice, there was a reduction in the number of prelocalized, postlocalized, and colocalized puncta depending on cochlear frequency/location (α9KO Control: n_{Apex} = 100 IHC, n_{Middle} = 84 IHC, n_{Base} = 118 IHC; α9KO Exposed: n_{Apex} = 234 IHC, n_{Middle} = 60 IHC, n_{Base} = 90 IHC). (**c**) In traumatized α9KI mice, no

difference was found in the number of presynaptic ribbons, postsynaptic AMPA receptors, and colocalization puncta for the three regions of the cochlea (α9KI Control: n_{Apex} = 178 IHC, n_{Middle} = 319 IHC, n_{Base} = 198 IHC; α9KI Exposed: n_{Apex} = 196 IHC, n_{Middle} = 145 IHC, n_{Base} = 80 IHC). Violin plots indicate median (solid line) and IQR (dashed lines). Asterisks denote the statistical significance (Mann Whitney test, **$p < 0.01$; ***$p < 0.001$, ****$p < 0.0001$).

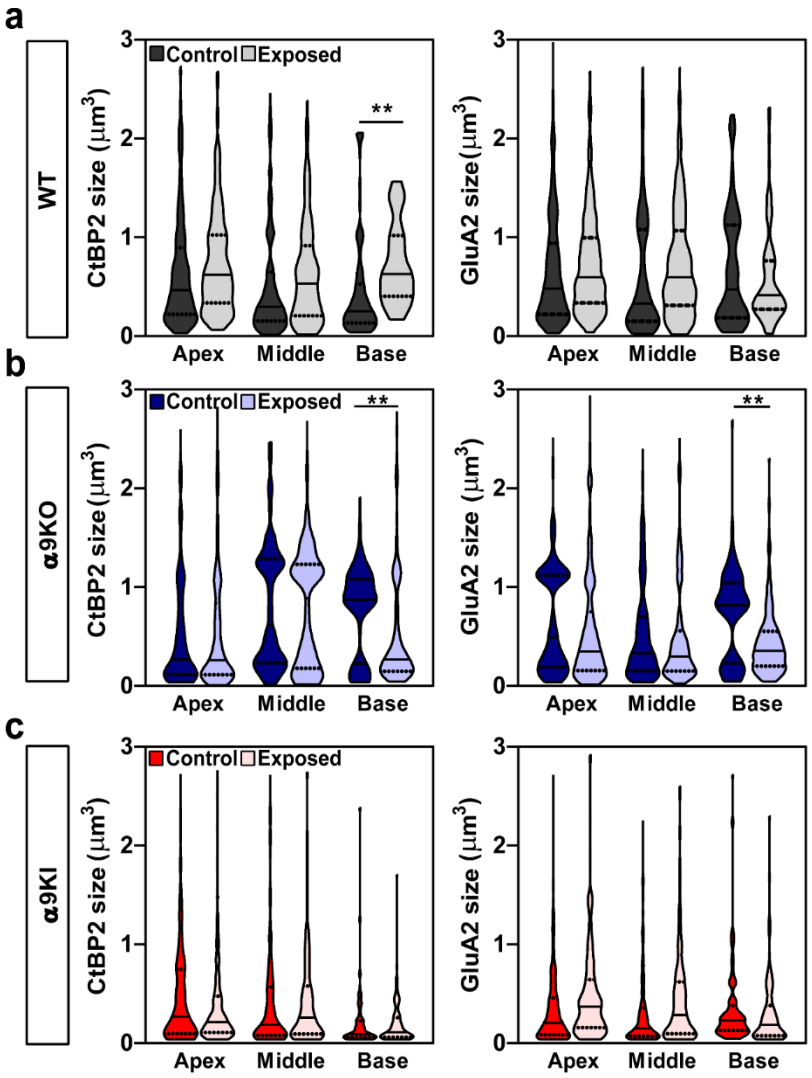

Figure 7: Volumes of presynaptic ribbons and postsynaptic receptor patches for each synaptic pair from control and noise-exposed WT, α9KO and α9KI mice. Violin plots comparing the volumes of fluorescence staining for ribbons (CtBP2 size) and AMPA receptors (GluA2 size) between control and noise-exposed mice. The quantification was made in the apex, middle and base regions of the cochlea from WT (**a**) (Control: n_{Apex} = 450 synaptic pairs, n_{Middle} = 509 synaptic pairs, n_{Base} = 203 synaptic pairs; Exposed: n_{Apex} = 497 synaptic pairs, n_{Middle} = 175 synaptic pairs, n_{Base} = 250 synaptic pairs); α9KO (**b**) (Control: n_{Apex} = 367 synaptic pairs, n_{Middle} = 187 synaptic pairs, n_{Base} = 221 synaptic pairs; Exposed: n_{Apex} = 207 synaptic pairs, n_{Middle} = 300 synaptic pairs, n_{Base} = 145 synaptic pairs) and α9KI (**c**) (Control: n_{Apex} = 247 synaptic pairs, n_{Middle} = 270 synaptic pairs, n_{Base} = 240 synaptic pairs; Exposed: n_{Apex} = 280 synaptic pairs, n_{Middle} = 310 synaptic pairs, n_{Base} = 360 synaptic pairs) mice. Violin plots indicate median (solid line) and IQR (dashed lines). Asterisks denote the statistical significance (t-test; *$p < 0.05$; ***$p < 0.001$).

SUPPLEMENTARY INFORMATION

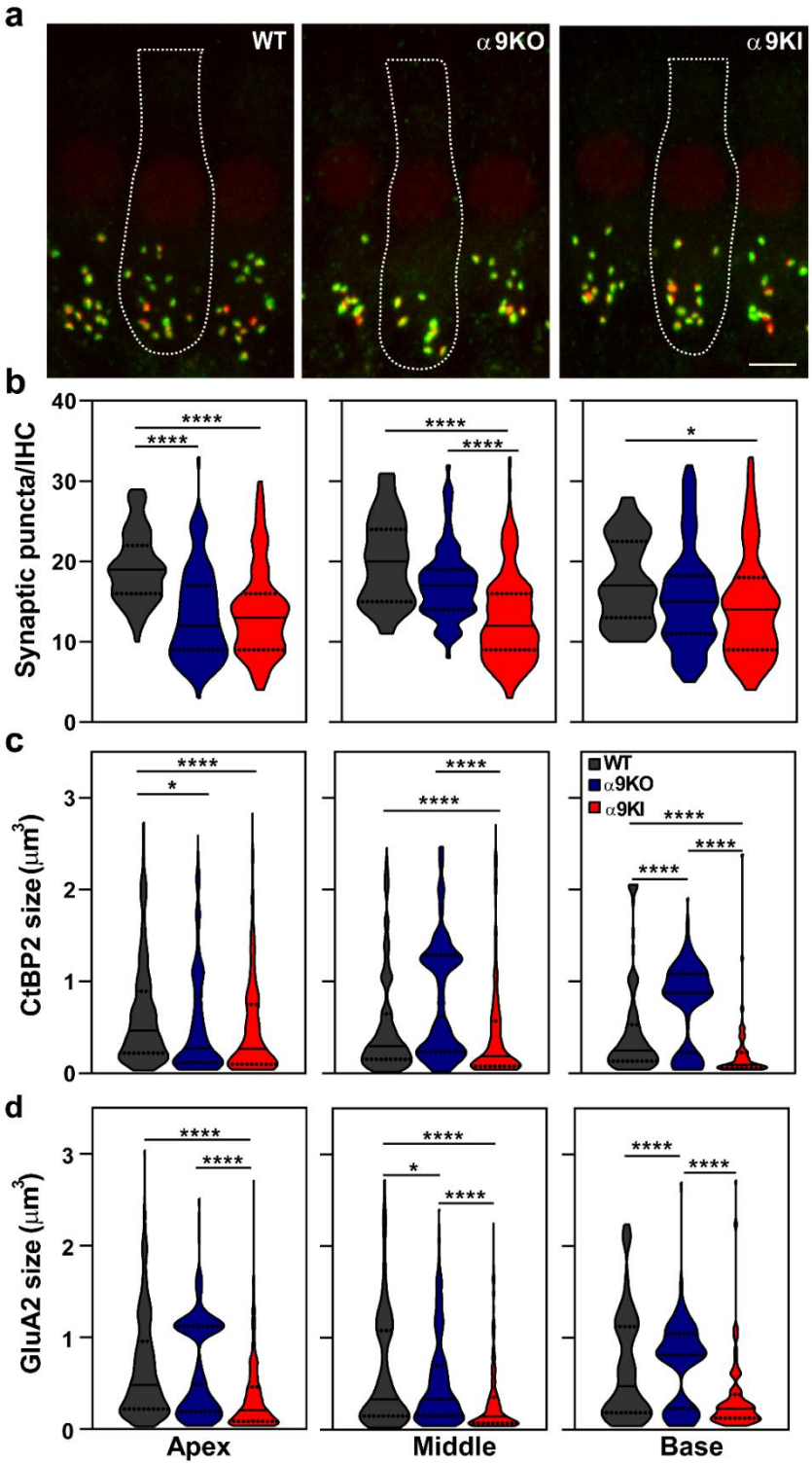

Supplementary Figure 1. Analysis of IHC ribbon synapses in unexposed WT, α9KO, and α9KI mice. (**a**) Representative confocal images of IHC synapses at the apex of the cochlea from

cochleae immunolabeled for presynaptic ribbons (CtBP2-red) and postsynaptic receptor patches (GluA2-green) for WT (left), α9KO (middle) and α9KI (right). CtBP2 antibody also weakly stains IHC nuclei. Scale bar, 7 µm. (**b**) Number of putative ribbon synapses per IHC (i.e., colocalized CtBP2 and GluA2 puncta). WT: n_{Apex} = 80 IHC, n_{Middle} = 75 IHC, n_{Base} = 60 IHC from 14 animals; α9KO: n_{Apex} = 100 IHC, n_{Middle} = 84 IHC, n_{Base} = 118 IHC from 11 animals and α9KI: n_{Apex} = 178 IHC, n_{Middle} = 319 IHC, n_{Base} = 198 IHC from 12 animals. (**c**) Volumes of fluorescence staining for ribbons (CtBP2 size) and (**d**) AMPA receptors (GluA2 size) for each of the synaptic pairs (WT: n_{Apex} = 450 synaptic pairs, n_{Middle} = 509 synaptic pairs, n_{Base} = 203 synaptic pairs; α9KO: n_{Apex} = 367 synaptic pairs, n_{Middle} = 187 synaptic pairs, n_{Base} = 221 synaptic pairs and α9KI: n_{Apex} = 247 synaptic pairs, n_{Middle} = 270 synaptic pairs, n_{Base} = 240 synaptic pairs). Violin plots indicate median (solid line) and interquartile range (IQR, dashed lines). Asterisks denote the statistical significance (Kruskal–Wallis followed by a Dunn's post-test was used to analyze the number of synapses and one way ANOVA followed by Holm-Sidak test; *$p < 0.05$; **$p < 0.01$; ***$p < 0.001$, ****$p < 0.0001$).

METHOD DETAILS

Animals. α9KO and α9KI mice have been previously described [42,45] and were backcrossed with the congenic FVB.129P2-*Pde6bþ Tyrc-ch/AntJ* strain (https://www.jax.org/strain/004828) for seventeen generations (i.e., N-17). We maintained a consistent male-to-female ratio across all experimental groups and genotypes. No sex-related differences were observed in the data. This study included adult and pup animals aged P12 to P16, which were housed in a sound-controlled room within the animal care facility. Background sound levels in this environment were consistently below 50 dB SPL. Noise levels were measured using an electret condenser microphone (FG-23329-PO7; Knowles). Transient sounds during routine cage cleaning and daily maintenance by animal care staff were minimal, with peaks not exceeding 70 dB SPL. The methods reported in this study adhere to the ARRIVE guidelines for reporting *in vivo* animal research (https://arriveguidelines.org/), ensuring transparency and reproducibility. All procedures were conducted in accordance with institutional and ethical guidelines for animal care and use.

Auditory function tests. Physiological assessments of cochlear and central function, including auditory brainstem responses (ABRs) and distortion-product otoacoustic emissions (DPOAEs), were performed in mice anesthetized with xylazine (10 mg/kg, i.p.) and ketamine (100 mg/kg, i.p.) and placed in a soundproof chamber maintained at 32°C to counteract the drop in body temperature caused by anesthesia. ABR represents sound-evoked potentials generated by neural circuits in the ascending auditory pathways, while DPOAEs are sounds emitted by the cochlea, specifically by OHCs, in response to two pure-tone stimuli presented simultaneously. Sound stimuli were delivered through a custom acoustic system with two dynamic earphones used as sound sources (CDMG15008–03A; CUI) and an electret condenser microphone (FG-23329-PO7; Knowles) coupled to a probe tube to measure sound pressure near the eardrum. Data collection was conducted using a National Instruments PXI-based system equipped with 24-

bit input/output boards and operated through a custom LabView software interface. For ABRs, platinum needle electrodes were placed into the skin at the dorsal midline close to the neural crest and pinna with a ground electrode near the tail. ABR potentials were evoked with 5 ms tone pips (0.5 ms rise-fall, with a $\cos^2$ envelope, at 40/s) delivered to the eardrum at log-spaced frequencies from 5.6 to 45.25 kHz. The response was amplified 10,000X with a 0.3–3 kHz passband. Sound level was raised in 5 dB steps from 20 to 80 dB sound pressure level (SPL). At each level, 1024 responses were averaged with alternated stimulus polarity. Threshold for ABR was defined as the lowest stimulus level (<80 dB SPL) at which a repeatable wave 1 could be identified in the response waveform. The ABR waves 1, 2 and 3 amplitudes were computed by off-line analysis of the peak-to-peak amplitude of stored waveforms. The DPOAEs in response to two primary tones of frequency f1 and f2 were recorded at 2f1-f2, with f2/f1=1.2, and the f2 level 10 dB lower than the f1 level. Ear-canal sound pressure was amplified and digitally sampled at 4 µs intervals. DPOAE threshold was defined as the lowest f2 level in which the signal to noise floor ratio is >1.

Noise exposure. Animals were exposed under anesthesia at P15 to a 1–16 kHz noise at 100 dB SPL for 1 hour using closed-field earphones (CDMG15008–03A; CUI) as the sound source. The exposure took place in the same acoustic chamber used for cochlear function tests. The noise consisted of a flat-spectrum broadband signal calibrated to the target SPL immediately before each exposure session.

Animal monitoring and health assessment. To assess the impact of repeated anesthesia on the health and well-being of the animals, their weight and motor activity were monitored daily throughout the auditory function recordings and noise exposure protocols. Animals were observed during their recovery from anesthesia to ensure no adverse effects on their general condition. Growth curves showed no significant differences in weight between animals that were

anesthetized and untreated controls animals, suggesting that anesthesia did not affect normal growth. Furthermore, no behavioral changes or motor impairments were observed in the anesthetized animals when compared to controls, indicating that repeated anesthesia had no detectable impact on overall health or behavior.

Cochlear processing and immunostaining. Cochleae were perfused intralabyrinthly with 4% paraformaldehyde (PFA) in phosphate-buffered saline (PBS), post-fixed with 4% PFA overnight, and decalcified in 0.12 M EDTA. Cochlear tissues were microdissected and permeabilized by freeze/thaw cycles in 30% sucrose. The dissected samples were then separated into distinct wells based on cochlear region: apex, middle and base. Tissue samples were blocked with 5% normal goat serum and 1% Triton X-100 in PBS for 1 h, followed by incubation in primary antibodies (diluted in blocking buffer) at 37°C for 16 h. The primary antibodies used in this study were: 1) anti-C-terminal binding protein 2 (mouse anti-CtBP2 IgG1; BD Biosciences, San Jose, CA; Cat#612044, RRID:AB_399431, 1:200) to label the presynaptic ribbon, 2) anti-glutamate receptor 2 (mouse anti-GluA2 IgG2a; Millipore, Billerica, MA; Cat#MAB397, RRID:AB_11212990, 1:2000) to label the post-synaptic receptor plaques and 3) anti-Myosin 7a (rabbit anti-MyosinVIIa, Proteus Biosciences; Cat# 25-6790, RRID:AB_10015251, 1:200) to label the cochlear hair cells. Tissues were then incubated with the appropriate Alexa Fluor-conjugated fluorescent secondary antibodies (Invitrogen, Carlsbad, CA; 1:500 in blocking buffer) for 2 hours at room temperature. Finally, tissues were mounted on microscope slides in FluorSave mounting media (Millipore, Billerica, MA).

Confocal microscopy and image processing. For IHC synaptic counts, cochlear tissue from the apex, middle and base regions was first imaged at low magnification to correlate each piece with its corresponding frequency region [88]. The apical region corresponds to 4–12 kHz, the

middle region to 12–20 kHz, and the base region to 22–40 kHz. Z-stacks images were then acquired using a Leica TCS SPE microscope with a 63X oil-immersion lens (1.5X or 4X digital zoom). Imaging settings were consistent across all samples, ensuring no pixel saturation. For each stack, the Z-step was set to 0.3 µm, with a pixel size of 0.11 µm in both the X and Y axes. Each stack typically contained 10 to 20 IHCs. Image stacks were processed using Fiji software (RRID:SCR_002285) [89], and a custom plugin was developed to automate the counting of synaptic ribbons, glutamate receptor patches and co-localized synaptic puncta. The algorithm's accuracy was validated by comparing automated counts to manual counts, ensuring reliable quantification. Briefly, each channel was analyzed separately, and maximum projections were generated to quantify the number of CtBP2 or GluA2 puncta. Additionally, a composite between the three channels was produced to draw the different regions of interest (ROI) that correspond to each IHC taking the myosin staining as a reference. The maximum projections from the single channels were multiplied to generate a merged 32-bit image. Then, they were converted to binary images after a custom thresholding procedure. An automatic counting of the number of particles on each ROI was performed.

For quantitative volumetric synaptic analysis, different regions from the whole cochlea were imaged and confocal z-stacks were processed in Fiji. z-stacks were deconvolved applying 10 iterations of the Richardson-Lucy algorithm in the DeconvolutionLab2 plugin [90], an algorithm that has been used previously in cochlear whole mounts [91]. Then, the 3D Object Counter plugin was used to perform three-dimensional image segmentation and object individualization of the deconvoluted stacks. According to previous work [58,92,93] we reasoned that a synapse would occupy a volume between 0.04 µm3 to 5 µm3, and then we set a size range of 20-2000 voxels, with a voxel size of 0.11 µm x 0.11 µm x 0.2 µm. The volumes of presynaptic ribbons (CtBP2 fluorescence) and postsynaptic AMPA receptor clusters (GluA2 fluorescence) at IHC-afferent synapses were measured using the 3D ROI Manager [94]. All exported volumes were checked to

ensure that volumes were within instrument resolution limits after threshold adjustments.

Statistical analysis

Data was analyzed using R Statistical Software (RRID:SCR_001905). Shapiro-Wilks test was used for testing normal distribution of the residuals. In cases where the data did not follow a normal distribution, the following tests were used: Kruskal-Wallis test followed by multiple contrasts according to Dunn's method for comparisons between three groups (IHCs synaptic counts in the control condition, ABR and DPOAE thresholds during development) and Mann-Whitney U test for comparisons between two groups (ABR thresholds, DPOAE thresholds, and IHCs synaptic counts). If data were normally distributed, a one-way ANOVA was conducted, followed by Holm-Sidak post hoc tests for three-group comparisons (wave 1 amplitudes and synaptic volumes in the control condition). For two-group comparisons, a t-test was used (synaptic volumes). Statistical significance was set to $p<0.05$.

REFERENCES

1. Sanes DH, Walsh EJ. The development of central auditory processing. In: Rubel EW, Popper AN, Fay RR, editors. Development of the Auditory System. New York: Springer; 1998. pp. 271–314.

2. Sanes DH, Bao S. Tuning up the developing auditory CNS. Curr Opin Neurobiol. 2009;19: 188–199. Available: http://www.ncbi.nlm.nih.gov/entrez/query.fcgi?cmd=Retrieve&db=PubMed&dopt=Citation&list_uids=19535241

3. Chang EF, Merzenich MM. Environmental noise retards auditory cortical development. Science. 2003;300: 498–502. doi:10.1126/science.1082163

4. Keuroghlian AS, Knudsen EI. Adaptive auditory plasticity in developing and adult animals. Prog Neurobiol. 2007;82: 109–121. doi:10.1016/j.pneurobio.2007.03.005

5. Zhou X, Merzenich MM. Enduring effects of early structured noise exposure on temporal modulation in the primary auditory cortex. Proc Natl Acad Sci U S A. 2008;105: 4423–4428. doi:10.1073/pnas.0800009105

752 6. Lauer AM, May BJ, Ay BRJM, Lauer AM, May BJ. The medial olivocochlear system attenuates the
753 developmental impact of early noise exposure. JARO - J Assoc Res Otolaryngol. 2011;12: 329–
754 343. doi:10.1007/s10162-011-0262-7

755 7. Caminos C, Vale E, Lujan R, Martinez-Galan JR, Juiz JM. Developmental regulation and adult
756 maintenance of potassium channel proteins (Kv 1.1 and Kv 1.2) in the cochlear nucleus of the rat.
757 Brain Res. 2005;1056. doi:10.1016/j.brainres.2005.07.031

758 8. Waguespack J, Salles FT, Kachar B, Ricci AJ. Stepwise morphological and functional maturation of
759 mechanotransduction in rat outer hair cells. J Neurosci Off J Soc Neurosci. 2007;27: 13890–
760 13902. doi:10.1523/JNEUROSCI.2159-07.2007

761 9. Dorrn AL, Yuan K, Barker AJ, Schreiner CE, Froemke RC. Developmental sensory experience
762 balances cortical excitation and inhibition. Nature. 2010;465: 932–936. doi:10.1038/nature09119

763 10. Sun YJ, Wu GK, Liu B-H, Li P, Zhou M, Xiao Z, et al. Fine-tuning of pre-balanced excitation and
764 inhibition during auditory cortical development. Nature. 2010;465: 927–931.
765 doi:10.1038/nature09079

766 11. Froemke RC, Jones BJ. Development of auditory cortical synaptic receptive fields. Neurosci
767 Biobehav Rev. 2011;35: 2105–2113. doi:10.1016/j.neubiorev.2011.02.006

768 12. Lippe WR. Rhythmic spontaneous activity in the developing avian auditory system. J Neurosci.
769 1994;14: 1486–1495. Available:
770 http://www.ncbi.nlm.nih.gov/entrez/query.fcgi?cmd=Retrieve&db=PubMed&dopt=Citation&list
771 _uids=8126550

772 13. Marcotti W, Johnson SL, Rusch A, Kros CJ. Sodium and calcium currents shape action potentials in
773 immature mouse inner hair cells. J Physiol. 2003;552: 743–761. Available:
774 http://www.ncbi.nlm.nih.gov/entrez/query.fcgi?cmd=Retrieve&db=PubMed&dopt=Citation&list
775 _uids=12937295

776 14. Sonntag M, Englitz B, Kopp-Scheinpflug C, Rübsamen R. Early Postnatal Development of
777 Spontaneous and Acoustically Evoked Discharge Activity of Principal Cells of the Medial Nucleus
778 of the Trapezoid Body: An In Vivo Study in Mice. J Neurosci. 2009;29: 9510–9520.
779 doi:10.1523/JNEUROSCI.1377-09.2009

780 15. Tritsch NX, Bergles DE. Developmental regulation of spontaneous activity in the Mammalian
781 cochlea. J Neurosci Off J Soc Neurosci. 2010;30: 1539–1550. doi:10.1523/JNEUROSCI.3875-
782 09.2010

783 16. Johnson SL, Eckrich T, Kuhn S, Zampini V, Franz C, Ranatunga KM, et al. Position-dependent
784 patterning of spontaneous action potentials in immature cochlear inner hair cells. Nat Neurosci.
785 2011;14: 711–717. doi:10.1038/nn.2803

786 17. De Faveri F, Ceriani F, Marcotti W. In vivo spontaneous Ca2+ activity in the pre-hearing
787 mammalian cochlea. Nat Commun. 2025;16: 29. doi:10.1038/s41467-024-55519-w

18. Tierney TS, Russell FA, Moore DR. Susceptibility of developing cochlear nucleus neurons to deafferentation-induced death abruptly ends just before the onset of hearing. J Comp Neurol. 1997;378: 295–306. doi:10.1002/(sici)1096-9861(19970210)378:2<295::aid-cne11>3.0.co;2-r

19. Friauf E, Lohmann C. Development of auditory brainstem circuitry. Activity-dependent and activity-independent processes. Cell Tissue Res. 1999;297: 187–195. doi:10.1007/s004410051346

20. Mostafapour SP, Cochran SL, Del Puerto NM, Rubel EW. Patterns of cell death in mouse anteroventral cochlear nucleus neurons after unilateral cochlea removal. J Comp Neurol. 2000;426: 561–571. doi:10.1002/1096-9861(20001030)426:4<561::aid-cne5>3.0.co;2-g

21. Leake PA, Hradek GT, Chair L, Snyder RL. Neonatal deafness results in degraded topographic specificity of auditory nerve projections to the cochlear nucleus in cats. J Comp Neurol. 2006;497: 13–31. doi:10.1002/cne.20968

22. Clause A, Kim G, Sonntag M, Weisz CJC, Vetter DE, Rűbsamen R, et al. The precise temporal pattern of prehearing spontaneous activity is necessary for tonotopic map refinement. Neuron. 2014;82: 822–835. doi:10.1016/j.neuron.2014.04.001

23. Di Guilmi MN, Boero LE, Castagna VC, Rodríguez-Contreras A, Wedemeyer C, Gómez-Casati ME, et al. Strengthening of the efferent olivocochlear system leads to synaptic dysfunction and tonotopy disruption of a central auditory nucleus. J Neurosci. 2019; 2536–18. doi:10.1523/jneurosci.2536-18.2019

24. Glowatzki E, Fuchs PA. Cholinergic synaptic inhibition of inner hair cells in the neonatal mammalian cochlea. Science. 2000;288: 2366–68.

25. Marcotti W, Johnson SL, Kros CJ. A transiently expressed SK current sustains and modulates action potential activity in immature mouse inner hair cells. J Physiol. 2004. Available: http://www.ncbi.nlm.nih.gov/entrez/query.fcgi?cmd=Retrieve&db=PubMed&dopt=Citation&list_uids=15331671

26. Goutman JD, Fuchs PA, Glowatzki E. Facilitating efferent inhibition of inner hair cells in the cochlea of the neonatal rat. J Physiol. 2005;566: 49–59. doi:10.1113/jphysiol.2005.087460

27. Johnson SL, Wedemeyer C, Vetter DE, Adachi R, Holley MC, Elgoyhen AB, et al. Cholinergic efferent synaptic transmission regulates the maturation of auditory hair cell ribbon synapses. Open Biol. 2013;3. doi:10.1098/rsob.130163

28. Wang Y, Sanghvi M, Gribizis A, Zhang Y, Song L, Morley B, et al. Efferent feedback controls bilateral auditory spontaneous activity. Nat Commun. 2021;12: 2449. doi:10.1038/s41467-021-22796-8

29. Walsh E, McGee J, McFadden S, Liberman M. Long-term effects of sectioning the olivocochlear bundle in neonatal cats. JNeurosci. 1998;18: 3859–3869.

30. Simmons DD, Mansdorf NB, Kim JH. Olivocochlear innervation of inner and outer hair cells during postnatal maturation: evidence for a waiting period. J Comp Neurol. 1996;370: 551–562. Available:

825 http://www.ncbi.nlm.nih.gov/entrez/query.fcgi?cmd=Retrieve&db=PubMed&dopt=Citation&list
826 _uids=8807454

827 31. Vattino LG, Wedemeyer C, Elgoyhen AB, Katz E. Functional Postnatal Maturation of the Medial
828 Olivocochlear Efferent–Outer Hair Cell Synapse. J Neurosci. 2020;40: 4842–4857.
829 doi:10.1523/JNEUROSCI.2409-19.2020

830 32. Wheeler EF, Bothwell M, Schecterson LC, von Bartheld CS. Expression of BDNF and NT-3 mRNA in
831 hair cells of the organ of Corti: quantitative analysis in developing rats. Hear Res. 1994;73: 46–56.

832 33. Ernfors P, Kucera J, Lee KF, Loring J, Jaenisch R. Studies on the physiological role of brain-derived
833 neurotrophic factor and neurotrophin-3 in knockout mice. Int J Dev Biol. 1995;39: 799–807.
834 Available:
835 http://www.ncbi.nlm.nih.gov/entrez/query.fcgi?cmd=Retrieve&db=PubMed&dopt=Citation&list
836 _uids=8645564

837 34. Knipper M, Zimmermann U, Rohbock K, Kopschall I, Zenner HP. Synaptophysin and GAP-43
838 proteins in efferent fibers of the inner ear during postnatal development. Brain Res Dev Brain
839 Res. 1995;89: 73–86. Available:
840 http://www.ncbi.nlm.nih.gov/entrez/query.fcgi?cmd=Retrieve&db=PubMed&dopt=Citation&list
841 _uids=8575095

842 35. Simmons DD, Manson-Gieseke L, Hendrix TW, McCarter S. Reconstructions of efferent fibers in
843 the postnatal hamster cochlea. Hear Res. 1990;49: 127–39.

844 36. Pujol R. Morphology, synaptology and electrophysiology of the developing cochlea. Acta
845 Otolaryngol Suppl. 1985;421: 5-9.

846 37. Pujol R, Carlier E, Devigne C. Different patterns of cochlear innervation during the development
847 of the kitten. J Comp Neurol. 1978;177: 529–36.

848 38. He DZ, Dallos P. Development of acetylcholine-induced responses in neonatal gerbil outer hair
849 cells. J Neurophysiol. 1999;81: 1162–1170. doi:10.1152/jn.1999.81.3.1162

850 39. Dulon D, Lenoir M. Cholinergic responses in developing outer hair cells of the rat cochlea. Eur J
851 Neurosci. 1996;8: 1945–1952.

852 40. Liberman MC. The olivocochlear efferent bundle and susceptibility of the inner ear to acoustic
853 injury. J Neurophysiol. 1991;65: 123–132. Available:
854 http://www.ncbi.nlm.nih.gov/entrez/query.fcgi?cmd=Retrieve&db=PubMed&dopt=Citation&list
855 _uids=1999726

856 41. Maison SF, Liberman MC. Predicting Vulnerability to Acoustic Injury with a Noninvasive Assay of
857 Olivocochlear Reflex Strength. J Neurosci. 2000;20: 4701–4707. doi:20/12/4701 [pii]

858 42. Taranda J, Maison SF, Ballestero JA, Katz E, Savino J, Vetter DE, et al. A point mutation in the hair
859 cell nicotinic cholinergic receptor prolongs cochlear inhibition and enhances noise protection.
860 PLoS Biol. 2009;7: 71–83. doi:10.1371/journal.pbio.1000018

861 43. Maison SF, Usubuchi H, Liberman MC. Efferent feedback minimizes cochlear neuropathy from
862 moderate noise exposure. J Neurosci. 2013;33: 5542–5552. doi:10.1523/jneurosci.5027-12.2013

863 44. Boero LE, Castagna VC, Di Guilmi MN, Goutman JD, Elgoyhen AB, Gómez-Casati ME.
864 Enhancement of the medial olivocochlear system prevents hidden hearing loss. J Neurosci.
865 2018;38: 7440–7451. doi:10.1523/JNEUROSCI.0363-18.2018

866 45. Vetter DE, Liberman MC, Mann J, Barhanin J, Boulter J, Brown MC, et al. Role of alpha9 nicotinic
867 ACh receptor subunits in the development and function of cochlear efferent innervation. Neuron.
868 1999;23: 93-103.

869 46. Buchwald JS, Huang CM. Far-field acoustic response: Origins in the cat. Science. 1975;189: 382–
870 384. doi:10.1126/science.1145206

871 47. Karplus M, Lee C, Cashore WJ, Oh W. The effects of brain bilirubin deposition on auditory brain
872 stem evoked responses in rats. Early Hum Dev. 1988;16: 185–194. doi:10.1016/0378-
873 3782(88)90098-9

874 48. Shapiro SM. Acute brainstem auditory evoked potential abnormalities in jaundiced Gunn rats
875 given sulfonamide. Pediatr Res. 1988;23: 306–310. doi:10.1203/00006450-198803000-00015

876 49. Shaw NA. The auditory evoked potential in the rat--a review. Prog Neurobiol. 1988;31: 19–45.
877 doi:10.1016/0301-0082(88)90021-4

878 50. Melcher J, Kiang NY. Generators of the brainstem auditory evoked potential in cat. III: Identified
879 cell populations. Hear Res. 1996;93: 52–71. doi:10.1016/0378-5955(95)00200-6

880 51. Kim SE, Turkington K, Kushmerick C, Kim JH. Central dysmyelination reduces the temporal fidelity
881 of synaptic transmission and the reliability of postsynaptic firing during high-frequency
882 stimulation. J Neurophysiol. 2013;110: 1621–1630. doi:10.1152/jn.00117.2013

883 52. Antoli-Candela FJ, Kiang N. Unit activity underlying the N1 potential. In: Naunton R, Fernandez C,
884 editors. Evoked electrical activity in the auditory nervous system. 1978. pp. 165–191.

885 53. Kujawa SG, Liberman MC. Adding insult to injury: cochlear nerve degeneration after “temporary”
886 noise-induced hearing loss. J Neurosci. 2009;29: 14077–14085. doi:10.1523/JNEUROSCI.2845-
887 09.2009

888 54. Shera CA, Guinan Jr. JJ. Evoked otoacoustic emissions arise by two fundamentally different
889 mechanisms: a taxonomy for mammalian OAEs. J Acoust Soc Am. 1999;105: 782–798.
890 doi:10.1121/1.426948.

891 55. Robles L, Ruggero MA. Mechanics of the mammalian cochlea. Physiol Rev. 2001;81: 1305–52.
892 doi:10.1152/physrev.2001.81.3.1305

893 56. Khimich D, Nouvian R, Pujol R, Tom Dieck S, Egner A, Gundelfinger ED, et al. Hair cell synaptic
894 ribbons are essential for synchronous auditory signalling. Nature. 2005;434: 889–894.
895 doi:10.1038/nature03393.

896 57. Matsubara A, Laake JH, Davanger S, Usami S, Ottersen OP. Organization of AMPA receptor
897 subunits at a glutamate synapse: a quantitative immunogold analysis of hair cell synapses in the
898 rat organ of Corti. J Neurosci. 1996;16: 4457–4467.

899 58. Liberman LD, Wang H, Liberman MC. Opposing gradients of ribbon size and AMPA receptor
900 expression underlie sensitivity differences among cochlear-nerve/hair-cell synapses. J Neurosci
901 Off J Soc Neurosci. 2011;31: 801–8. doi:10.1523/JNEUROSCI.3389-10.2011

902 59. Sendin G, Bourien J, Rassendren F, Puel J-L, Nouvian R. Spatiotemporal pattern of action potential
903 firing in developing inner hair cells of the mouse cochlea. Proc Natl Acad Sci U S A. 2014;111:
904 1999–2004. doi:10.1073/pnas.1319615111

905 60. Hirtz JJ, Boesen M, Braun N, Deitmer JW, Kramer F, Lohr C, et al. Cav1.3 calcium channels are
906 required for normal development of the auditory brainstem. J Neurosci Off J Soc Neurosci.
907 2011;31: 8280–8294. doi:10.1523/JNEUROSCI.5098-10.2011

908 61. Babola TA, Li S, Wang Z, Kersbergen CJ, Elgoyhen AB, Coate TM, et al. Purinergic Signaling
909 Controls Spontaneous Activity in the Auditory System throughout Early Development. J Neurosci
910 Off J Soc Neurosci. 2021;41: 594–612. doi:10.1523/JNEUROSCI.2178-20.2020

911 62. Frank T, Khimich D, Neef A, Moser T. Mechanisms contributing to synaptic Ca2+ signals and their
912 heterogeneity in hair cells. Proc Natl Acad Sci U S A. 2009;106: 4483–4488.
913 doi:10.1073/pnas.0813213106

914 63. Sheets L, Kindt KS, Nicolson T. Presynaptic CaV1.3 channels regulate synaptic ribbon size and are
915 required for synaptic maintenance in sensory hair cells. J Neurosci Off J Soc Neurosci. 2012;32:
916 17273–17286. doi:10.1523/JNEUROSCI.3005-12.2012

917 64. Wong HC, Zhang Q, Beirl AJ, Petralia RS, Wang Y-X, Kindt K. Synaptic mitochondria regulate hair-
918 cell synapse size and function. eLife. 2019;8: e48914. doi:10.7554/eLife.48914

919 65. Özçete ÖD, Moser T. A sensory cell diversifies its output by varying Ca2+ influx-release coupling
920 among active zones. EMBO J. 2021;40: e106010. doi:10.15252/embj.2020106010

921 66. Michanski S, Smaluch K, Maria Steyer A, Chakrabarti R, Setz C, Oestreicher D, et al. Mapping
922 developmental maturation of inner hair cell ribbon synapses in the apical mouse cochlea. Proc
923 Natl Acad Sci U S A. 2019;116: 6415–6424. doi:10.1073/pnas.1812029116

924 67. Hua Y, Ding X, Wang H, Wang F, Lu Y, Neef J, et al. Electron Microscopic Reconstruction of Neural
925 Circuitry in the Cochlea. Cell Rep. 2021;34: 108551. doi:10.1016/j.celrep.2020.108551

926 68. Payne SA, Joens MS, Chung H, Skigen N, Frank A, Gattani S, et al. Maturation of Heterogeneity in
927 Afferent Synapse Ultrastructure in the Mouse Cochlea. Front Synaptic Neurosci. 2021;13: 678575.
928 doi:10.3389/fnsyn.2021.678575

929 69. Sobkowicz HM, Rose JE, Scott GE, Slapnick SM. Ribbon synapses in the developing intact and
930 cultured organ of Corti in the mouse. J Neurosci. 1982;2: 942–57.

931 70. Merchan-Perez A, Liberman MC. Ultrastructural differences among afferent synapses on cochlear
932 hair cells: correlations with spontaneous discharge rate. J Comp Neurol. 1996;371: 208–221.
933 doi:10.1002/(SICI)1096-9861(19960722)371:2<208::AID-CNE2>3.0.CO;2-6

934 71. Huang L-C, Barclay M, Lee K, Peter S, Housley GD, Thorne PR, et al. Synaptic profiles during
935 neurite extension, refinement and retraction in the developing cochlea. Neural Develop. 2012;7:
936 38. doi:10.1186/1749-8104-7-38

937 72. Wong AB, Rutherford MA, Gabrielaitis M, Pangršič T, Göttfert F, Frank T, et al. Developmental
938 refinement of hair cell synapses tightens the coupling of Ca2+ influx to exocytosis. EMBO J.
939 2014;33: 247–264. doi:10.1002/embj.201387110

940 73. Song L, McGee J, Walsh EJ. Frequency- and level-dependent changes in auditory brainstem
941 responses (ABRS) in developing mice. J Acoust Soc Am. 2006;119: 2242–2257.
942 doi:10.1121/1.2180533

943 74. Fernandez KA, Jeffers PWC, Lall K, Liberman MC, Kujawa SG. Aging after noise exposure :
944 Acceleration of cochlear synaptopathy in “ recovered ” ears. J Neurosci. 2015;35: 7509–20.
945 doi:10.1523/JNEUROSCI.5138-14.2015

946 75. Schrode KM, Dent ML, Lauer AM. Sources of variability in auditory brainstem response thresholds
947 in a mouse model of noise-induced hearing loss. J Acoust Soc Am. 2022;152: 3576–3582.
948 doi:10.1121/10.0016593

949 76. Lu Y, Liu J, Li B, Wang H, Wang F, Wang S, et al. Spatial patterns of noise-induced inner hair cell
950 ribbon loss in the mouse mid-cochlea. iScience. 2024;27: 108825. doi:10.1016/j.isci.2024.108825

951 77. Rybalko N, Chumak T, Bureš Z, Popelář J, Šuta D, Syka J. Development of the acoustic startle
952 response in rats and its change after early acoustic trauma. Behav Brain Res. 2015;286: 212–221.
953 doi:10.1016/j.bbr.2015.02.046

954 78. Mohamad NI, Santra P, Park Y, Matthews IR, Taketa E, Chan DK. Synaptic ribbon dynamics after
955 noise exposure in the hearing cochlea. Commun Biol. 2024;7: 421. doi:10.1038/s42003-024-
956 06067-y

957 79. Moverman DJ, Liberman LD, Kraemer S, Corfas G, Liberman MC. Ultrastructure of noise-induced
958 cochlear synaptopathy. Sci Rep. 2023;13: 19456. doi:10.1038/s41598-023-46859-6

959 80. Stamataki S, Francis HW, Lehar M, May BJ, Ryugo DK. Synaptic alterations at inner hair cells
960 precede spiral ganglion cell loss in aging C57BL/6J mice. Hear Res. 2006;221: 104–118.
961 doi:10.1016/j.heares.2006.07.014

962 81. Jeng JY, Ceriani F, Olt J, Brown SDM, Holley MC, Bowl MR, et al. Pathophysiological changes in
963 inner hair cell ribbon synapses in the ageing mammalian cochlea. J Physiol. 2020;598: 4339–4355.
964 doi:10.1113/JP280018

965 82. Boero LE, Payne S, Gómez-Casati ME, Rutherford MA, Goutman JD. Noise Exposure Potentiates
966 Exocytosis From Cochlear Inner Hair Cells. Front Synaptic Neurosci. 2021;13: 740368.
967 doi:10.3389/fnsyn.2021.740368

968 83. Suthakar K, Liberman MC. Auditory-Nerve Responses in Mice with Noise-Induced Cochlear
969 Synaptopathy. https://doi.org/101152/jn003422021. 2021 [cited 24 Nov 2021].
970 doi:10.1152/JN.00342.2021

971 84. Wood MB, Nowak N, Mull K, Goldring A, Lehar M, Fuchs PA. Acoustic Trauma Increases Ribbon
972 Number and Size in Outer Hair Cells of the Mouse Cochlea. J Assoc Res Otolaryngol JARO.
973 2021;22: 19–31. doi:10.1007/s10162-020-00777-w

974 85. Furman AC, Kujawa SG, Liberman MC. Noise-induced cochlear neuropathy is selective for fibers
975 with low spontaneous rates. J Neurophysiol. 2013;110: 577–586. doi:10.1152/jn.00164.2013

976 86. Benini F, Magnavita V, Lago P, Arslan E, Pisan P. Evaluation of noise in the neonatal intensive care
977 unit. Am J Perinatol. 1996;13: 37–41. doi:10.1055/s-2007-994200

978 87. Lahav A, Skoe E. An acoustic gap between the NICU and womb: a potential risk for compromised
979 neuroplasticity of the auditory system in preterm infants. Front Neurosci. 2014;8: 381.
980 doi:10.3389/fnins.2014.00381

981 88. Muller M, von Hunerbein K, Hoidis S, Smolders JW. A physiological place-frequency map of the
982 cochlea in the CBA/J mouse. Hear Res. 2005;202: 63–73. Available:
983 http://www.ncbi.nlm.nih.gov/entrez/query.fcgi?cmd=Retrieve&db=PubMed&dopt=Citation&list
984 _uids=15811700

985 89. Schindelin J, Arganda-Carreras I, Frise E, Kaynig V, Longair M, Pietzsch T, et al. Fiji: an open-source
986 platform for biological-image analysis. Nat Methods. 2012;9: 676–82. doi:10.1038/nmeth.2019

987 90. Sage D, Donati L, Soulez F, Fortun D, Schmit G, Seitz A, et al. DeconvolutionLab2: An open-source
988 software for deconvolution microscopy. Methods. 2017;115: 28–41.
989 doi:10.1016/j.ymeth.2016.12.015

990 91. Jing Z, Rutherford MA, Takago H, Frank T, Fejtova A, Khimich D, et al. Disruption of the
991 presynaptic cytomatrix protein bassoon degrades ribbon anchorage, multiquantal release, and
992 sound encoding at the hair cell afferent synapse. J Neurosci. 2013;33: 4456–4467.
993 doi:10.1523/JNEUROSCI.3491-12.2013

994 92. Gilels F, Paquette ST, Zhang J, Rahman I, White PM. Mutation of foxo3 causes adult onset
995 auditory neuropathy and alters cochlear synapse architecture in mice. J Neurosci. 2013;33:
996 18409–18424. doi:10.1523/JNEUROSCI.2529-13.2013

997 93. Paquette ST, Gilels F, White PM. Noise exposure modulates cochlear inner hair cell ribbon
998 volumes, correlating with changes in auditory measures in the FVB/nJ mouse. Sci Rep. 2016;6: 1–
999 13. doi:10.1038/srep25056

1000 94. Ollion J, Cochennec J, Loll F, Escudé C, Boudier T. TANGO: A generic tool for high-throughput 3D
1001 image analysis for studying nuclear organization. Bioinformatics. 2013;29: 1840–1841.
1002 doi:10.1093/bioinformatics/btt276

1003

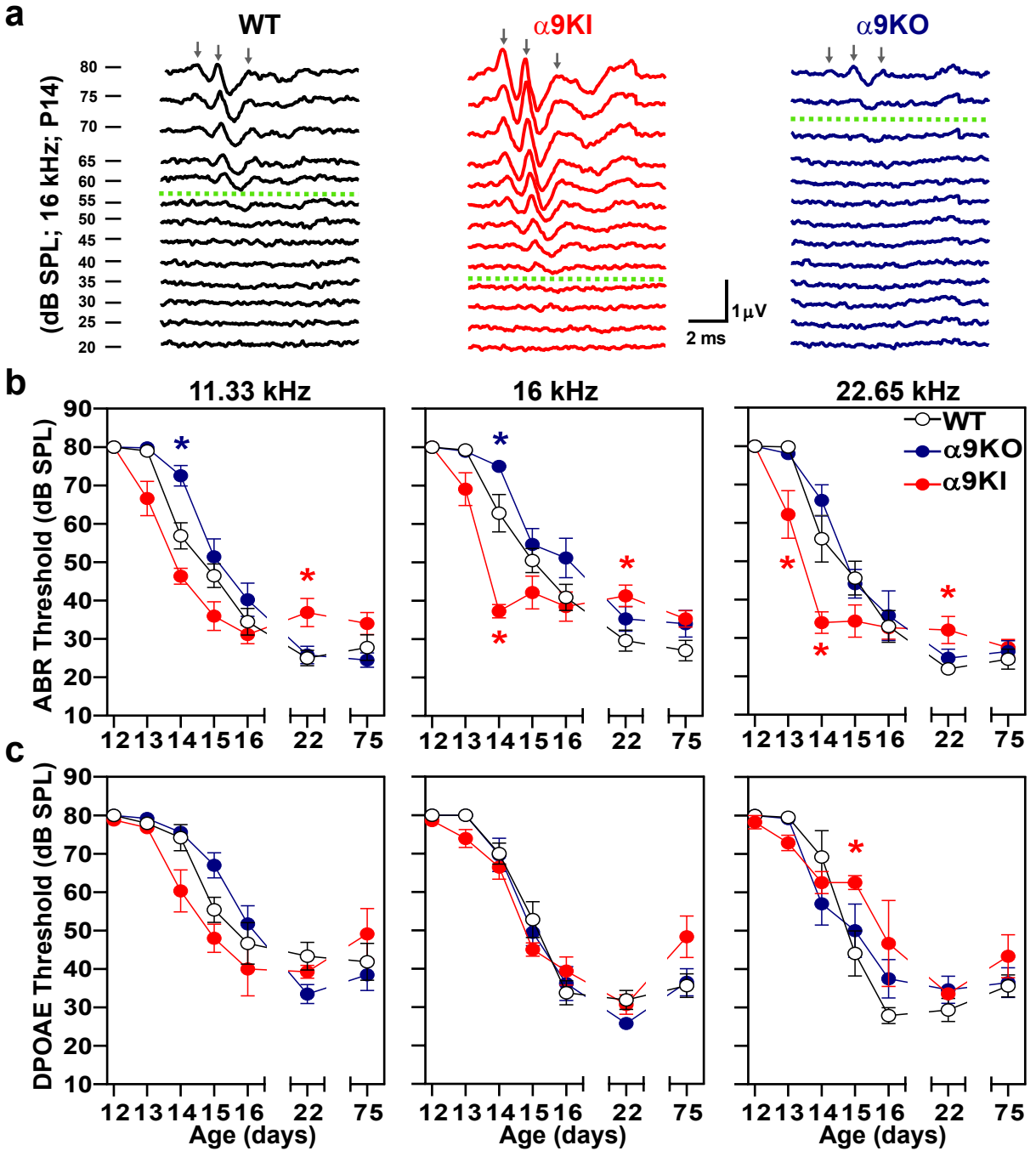
a
WT
α9KI
α9KO
(dB SPL; 16 kHz; P14)
80
75
70
65
60
55
50
45
40
35
30
25
20
1 μV
2 ms
b
11.33 kHz
16 kHz
22.65 kHz
WT
α9KO
α9KI
ABR Threshold (dB SPL)
90
80
70
60
50
40
30
20
10
12 13 14 15 16 22 75
c
DPOAE Threshold (dB SPL)
Age (days)

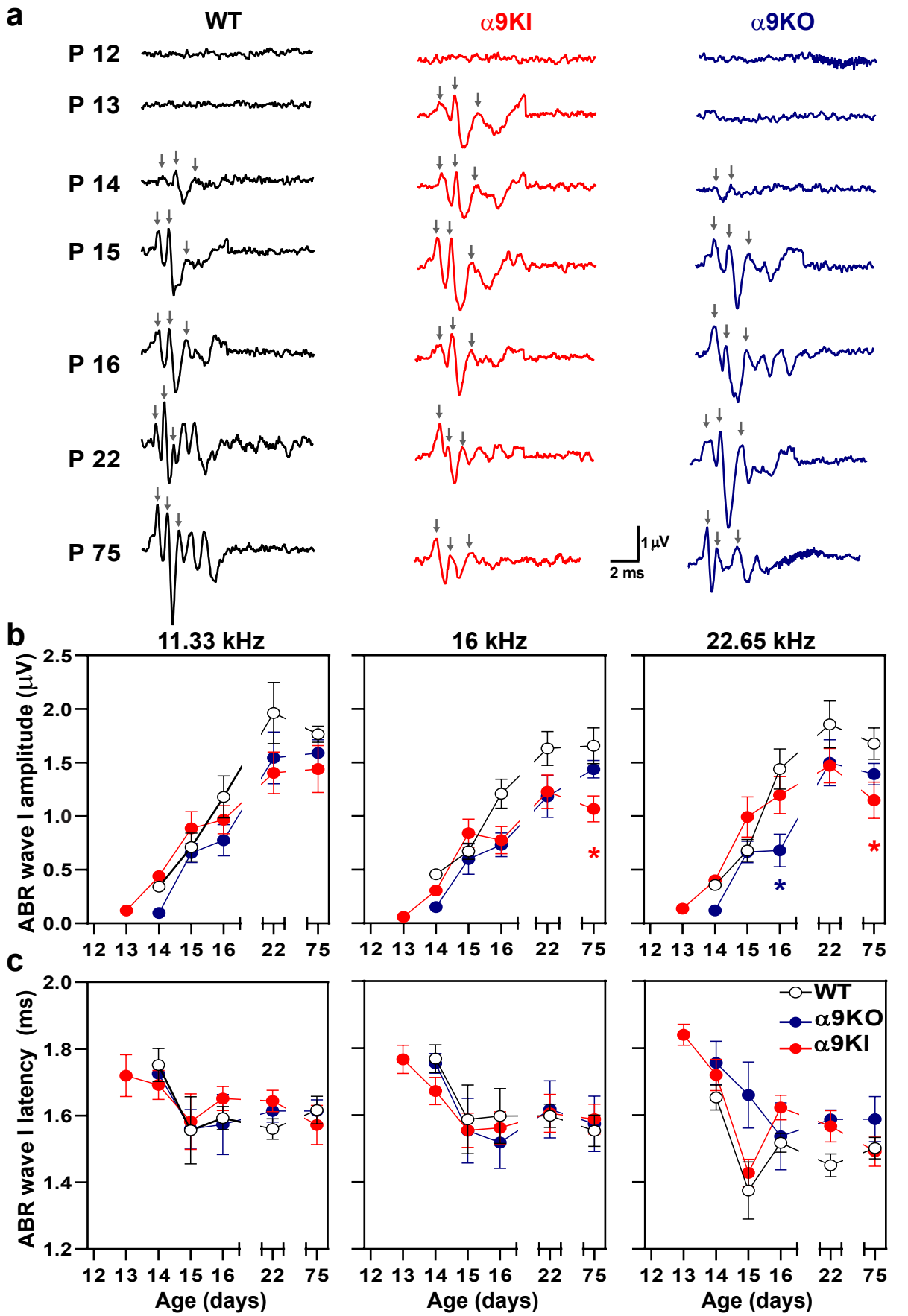
a
WT
α9KI
α9KO
P 12
P 13
P 14
P 15
P 16
P 22
P 75
1 μV
2 ms
b
11.33 kHz
16 kHz
22.65 kHz
ABR wave I amplitude (μV)
2.5
2.0
1.5
1.0
0.5
0.0
12 13 14 15 16 22 75
c
ABR wave I latency (ms)
2.0
1.8
1.6
1.4
1.2
Age (days)
WT
α9KO
α9KI

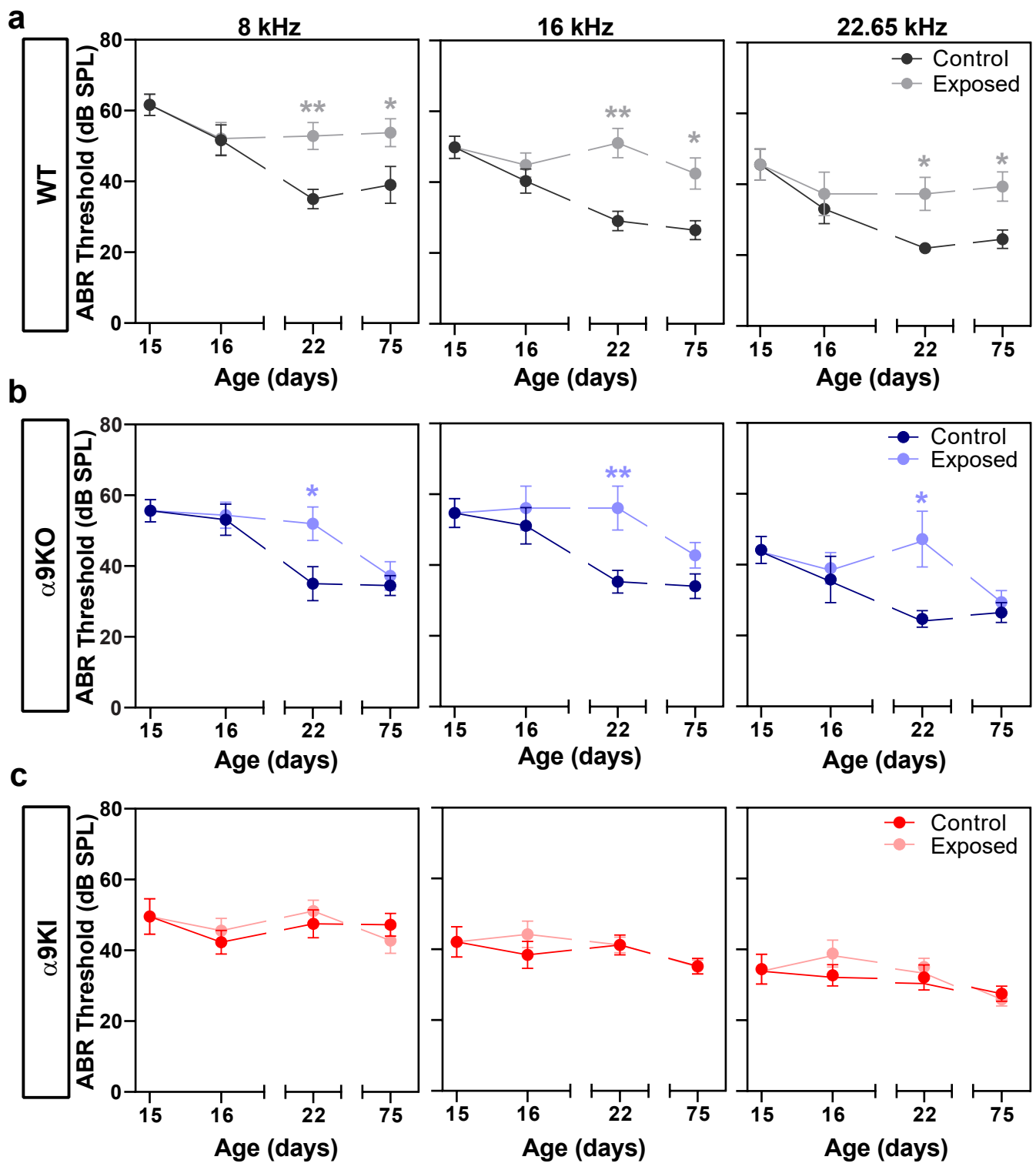
a
8 kHz
16 kHz
22.65 kHz
WT
ABR Threshold (dB SPL)
Control
Exposed
**
*
Age (days)
b
α9KO
c
α9KI
0
20
40
60
80
15
16
22
75

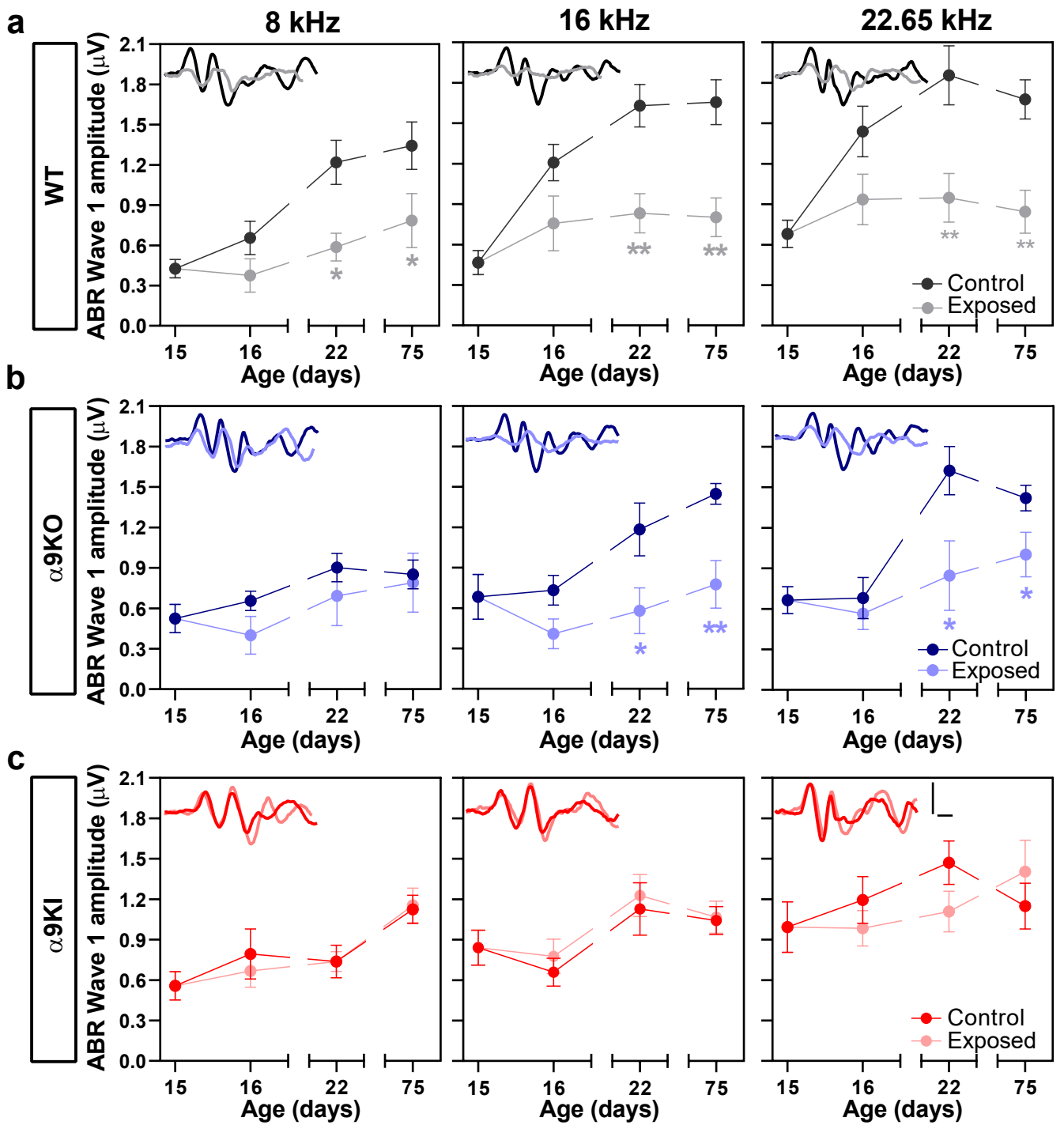
a
8 kHz
16 kHz
22.65 kHz
WT
ABR Wave 1 amplitude (μV)
2.1
1.8
1.5
1.2
0.9
0.6
0.3
0.0
15
16
22
75
Age (days)
*
**
Control
Exposed
b
α9KO
c
α9KI

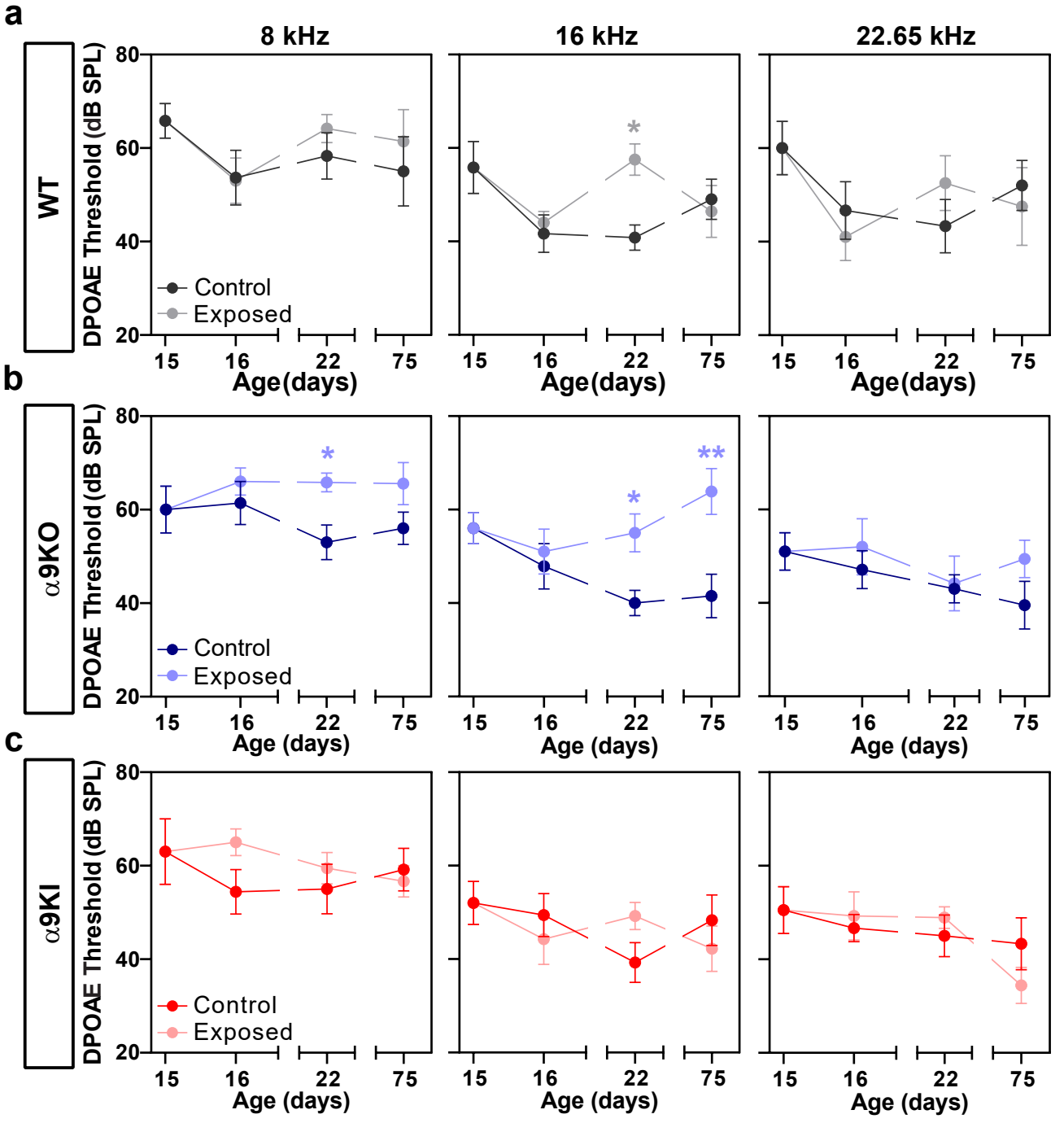
a
8 kHz
16 kHz
22.65 kHz
WT
DPOAE Threshold (dB SPL)
80
60
40
20
Control
Exposed
*
15
16
22
75
Age(days)
b
α9KO
Control
Exposed
*
*
**
Age (days)
c
α9KI
Control
Exposed
Age (days)

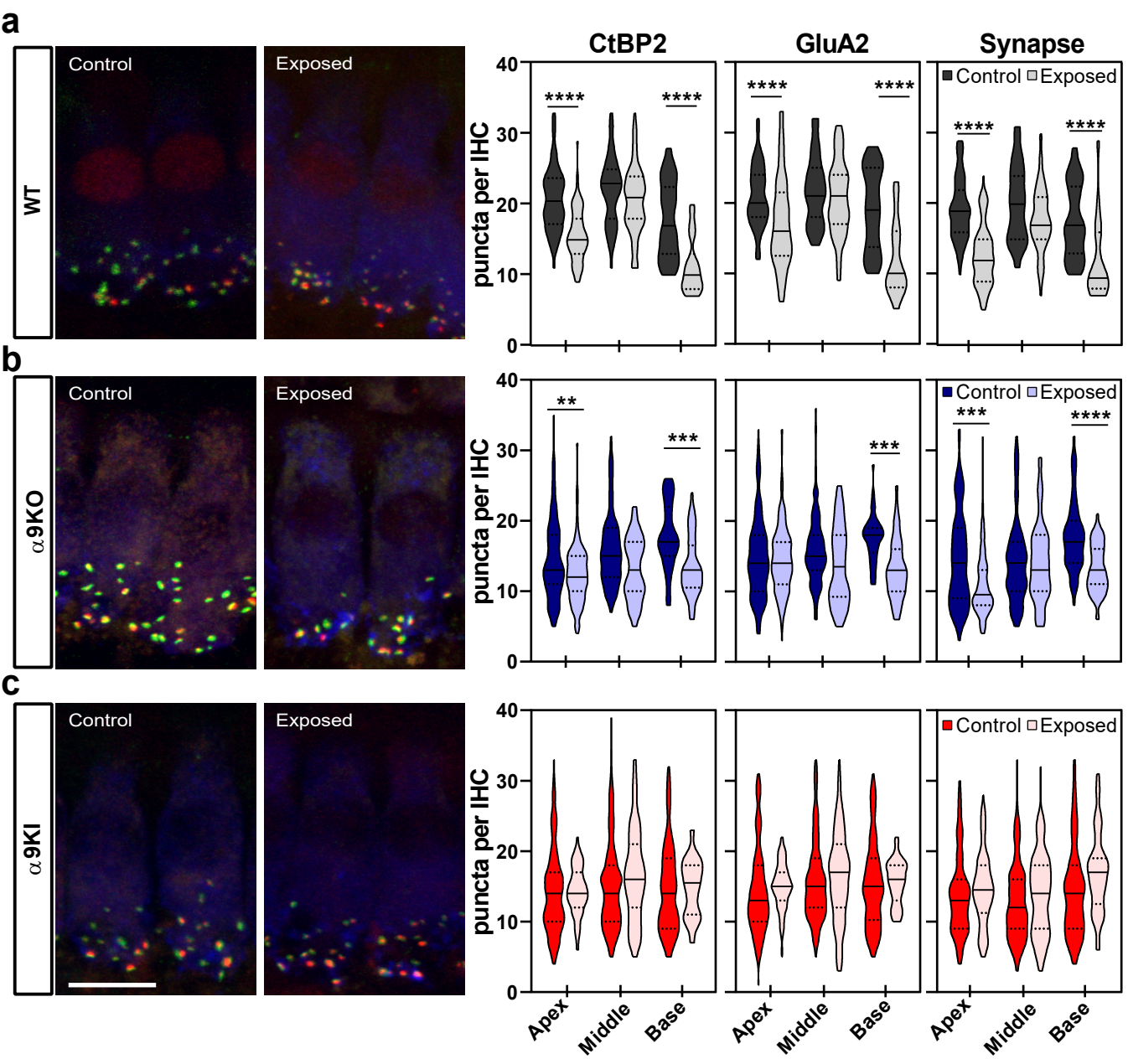
a
b
c
WT
α9KO
α9KI
Control
Exposed
CtBP2
GluA2
Synapse
puncta per IHC
0
10
20
30
40
****
**
***
Apex
Middle
Base

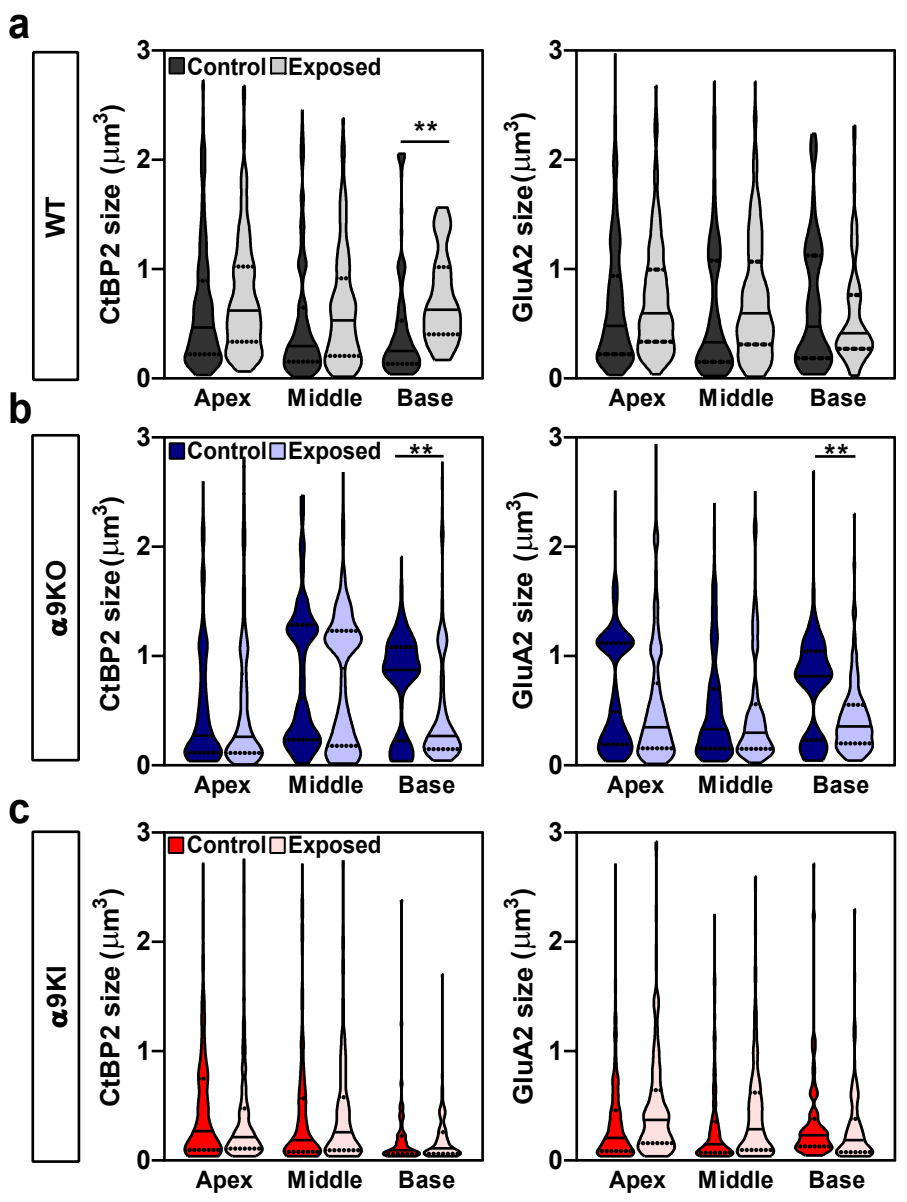
a
WT
Control
Exposed
CtBP2 size (μm3)
GluA2 size (μm3)
**
Apex
Middle
Base
b
α9KO
Control
Exposed
CtBP2 size (μm3)
GluA2 size (μm3)
**
**
Apex
Middle
Base
c
α9KI
Control
Exposed
CtBP2 size (μm3)
GluA2 size (μm3)
Apex
Middle
Base